LEVEL (8)

(9) Rept for 1 May — 1∅ Nov 63

(6) STRESS AND FATIGUE ANALYSIS
QRC-335A POD.

Revision C.

(11) 1∅ NOV [redacted]63

Albert B. Simon

(12) 136p.

(15) F [illegible]

375 505

PAGES ______

ARE

MISSING

IN

ORIGINAL

DOCUMENT

FOREWORD

This report consists of a load and stress analysis of the QRC-335A pod. The analysis described was performed by the Westinghouse Defense and Space Center, Aerospace Division, Baltimore, Maryland, in accordance with the requirements of Air Force Contract No. F33657-67-C-0994.

Effort was devoted to the analysis from 1 March 1967 to 1 May 1967. Effort was devoted to Revision A from 26 June 1967 to 30 June 1967. Effort was devoted to Revision B from 20 November 1967 to 12 January 1968. Effort was devoted to Revision C from 1 May 1968 to 10 November 1968.

This report contains no classified information extracted from other classified documents.

ABSTRACT

This report presents the results of a load and stress analysis made on the primary structure of the QRC-335A pod. The methods of stress analysis stem largely from previous tests and analyses made on virtually identical structures. The McDonnell Company furnished load data which was reduced to establish the flight loads for the QRC-160-8 pod on the F-4C pylon at BL = 81.50 inches, and the Sparrow III 6B installed semisubmerged in the forward fuselage of the F-4C aircraft. The analysis shows that adequate margins of safety were obtained for these loads. Considering growth potential, some higher loads, called "integration loads," have been included to depict the worst case that would be encountered on the F-111A, F-4C, and F-105 aircraft. These loads have also been used to calculate the margins of safety which were found to be adequate. Because of conservation in the weight calculations, load analysis, and stress analysis, the margins of safety are likewise conservative.

TABLE OF CONTENTS

TABLE OF CONTENTS (Continued)

TABLE OF CONTENTS (Continued)

LIST OF ILLUSTRATIONS

LIST OF TABLES

LIST OF TABLES (Continued)

LIST OF SYMBOLS

Symbol	Meaning	Units
$A_{(j)}$	function of neutral axis position	$in.^2$
A_b	bearing area of rivet	$in.^2$
A_t	net skin tension area per inch of circumference	in.
A_2	cross section area of skin	$in.^2$
A_3	cross section area of hardback	$in.^2$
A_4	cross section area of longeron	$in.^2$
BM	bending moment	in.-lb.
B_x	divisor of R_x for lug screw stress	$in.^2$
B_y	divisor of R_y for lug screw stress	$in.^2$
B_z	divisor of R_z for lug screw stress	$in.^2$
C	lug height to point that reacts axial loads above surface described by R	in.
CIN	stress difference coefficient (inside of skin)	stress/load
COUT	stress difference coefficient (outside of skin)	stress/load
CTAU	longitudinal shear-stress coefficient	stress/load
CTU	degradation factor for ultimate strength at elevated temperature	—
CTY	degradation factor for yield strength at elevated temperature	—
C_1	correction factor for plane stress	—
C_2	correction factor for bending stress	—
D	aerodynamic drag	lb.
D_r	nominal rivet diameter	in.
D_s	average distance of screws from N. A.	in.
d_{circ}	infinitesimal circumferential length	in.
d_{xi}	x distance of i_{th} bolt from edge of lug	in.

LIST OF SYMBOLS (Continued)

Symbol	Meaning	Units
d_{yi}	y distance of i_{th} bolt from edge of lug	in.
E	modulus of elasticity	lb/in^2
E	vertical distance from pod c.g. to origin of R	in.
FFU	room temperature ultimate strength	$lb/in.^2$
FFY	room temperature yield strength	lb/in^2
FT	stress or load at a point in the pod	various
F_{br}	allowable bearing stress in skin	lb/in^2
F_{bru}	bearing ultimate strength	lb/in^2
F_{bry}	bearing yield strength	lb/in^2
F_{bu}	modulus of rupture	lb/in^2
F_{cy}	compressive yield strength	lb/in^2
F_{su}	shear ultimate strength	lb/in^2
F_{tu}	tensile ultimate strength	lb/in^2
F_{ty}	tensile yield strength	lb/in^2
f	strain required in plastic to produce a fringe (photoelastic)	—
G	distance from nose to pod center	in.
H	lug height to point that reacts side loads above surface defined by R	in.
HI	distance from pod surface to surface described by R	in.
H_r	depth of countersink on screws or rivets	in.
I	area or mass moment of inertia	$in.^4$
I'_x	$\sum (d_{xi})^2$	$in.^2$
I'_y	$\sum (d_{yi})^2$	$in.^2$
i	subscript to denote a component of load such as vertical force, side force, pitching moment, etc.	—

Symbol	Meaning	Units
j	subscript to denote a critical stress area	--
K	a scale factor	--
KEY	correction factor to make computed yield strength agree with test results	--
KEU	correction factor to make computed ultimate strength agree with test results	--
L	general - load component such as side force, pitching moment, etc.	--
L	specific - aerodynamic lift	lb.
LA	aft lug distance from c. g.	in.
LAB	aft sway brace distance from c.g.	in.
LF	forward lug distance from c. g.	in.
LFB	forward sway brace distance from c. g.	in.
M	Mach no.	--
MSU	margin of safety, ultimate load, room temp.	--
MSUT	margin of safety, ultimate load, elevated temp.	--
MSY	margin of safety, limit load, room temp.	--
MSYT	margin of safety, limit load, elevated temp.	--
M_u	ultimate bending moment	in-lb.
M_x	total moment on pod about roll axis (thru c.g.), + bottom to port	in-lb.
M_y	total moment on pod about pitch axis (thru c.g.) + nose up	in-lb.
M_z	total moment on pod about yaw axis (thru c.g.) + nose to port	in-lb.
N	fringe order (photoelastic)	--
N_s	number of screws at a joint	--
N_t	axial force per inch of circumference	lb/in.
N_w	number of rows of rivets	--

LIST OF SYMBOLS (Continued)

Symbol	Meaning	Units
N_z	aircraft vertical acceleration, + up	g's
n_x	axial load factor, + aft	g's
n_y	lateral load factor, + port	g's
n_z	vertical load factors, + up	g's
n	pitching load factor, + nose up	rad/sec^2
n_x	yawing load factor, + nose to port	rad/sec^2
PM	aerodynamic pitching moment about geometric center, + nose up	in-lb.
PM'	aerodynamic pitching moment about original reference point, + nose up	in-lb.
PSX	fore and aft load that would yield lug	lb.
PSY	side load that would yield lug	lb.
PSZ	vertical load that would yield lug	lb.
P_{br}	bearing force of a rivet	lb.
P_r	compressive reaction at V-band clamp	lb.
P_s	shear load capability of rivets	lb.
P_{ss}	shear load capability of screws	lb.
P_u	ultimate failure load of lug	lb.
P_x	total axial load on pod at c.g., + aft	lb.
P_y	total side load on pod at c.g., + port	lb.
P_{yd}	yield failure load of lug	lb.
P_z	total vertical load on pod at c.g., + up	lb.
p	roll velocity	deg/sec
$\dot{p}$	roll acceleration	rad/sec^2
Q_s	ratio of skin moment of inertia to total moment of inertia (about N.A.)	—

Symbol	Meaning	Unit
Q_2	skin moment of inertia about centerline	in^4
Q_3	horizontal moment of inertia of hardback	in^4
Q_4	horizontal moment of inertia of longeron	in^4
Q_5	vertical moment of inertia of hardback about pod center	in^4
Q_6	vertical moment of inertia of longeron about pod center	in^4
R	length of normal line from sway brace contact point to intersection with vertical centerline (equals pod radius when no sway brace pad is used)	in
RM	aerodynamic rolling moment about c.g.	in-lb
R_b	stress ratio of bending stress in button	—
R_r	radius to contact of ring and clamp	in.
R_s	radius to shear interface(rivets)	in.
R_t	stress ratio of tensile stress in button	—
R_{ult}	overall stress ratio in button	—
R_x	axial lug reaction	lb.
R_y	side lug reaction	lb.
R_z	vertical lug reaction	lb.
R'_y, R'_z	lug reactions rotated to coordinate system thru center of book bolts	lb
r_1	radius of button shank	in
S	aerodynamic side force	lb.
SFU	ultimate safety factor (1.50)	—
SFY	yield safety factor (1.15)	—
SUMIN	summation of stress differences at a point on inside surface of skin	lb/in^2

LIST OF SYMBOLS (Continued)

Symbol	Meaning	Units
SUMOUT	summation of stress difference at a point on outside of skin	lb/in^2
SUMTAU	summation of shear stresses at a point	lb/in^2
S_c	spacing of rivets	in.
S_1	length of negligible mass at forward end	in.
S_2	length of negligible mass at aft end	in.
T_o	thickness of root of ring or clamp	in.
T_s	thickness of skin	in.
U	distance from point of contact to neutral axis in root of ring or clamp	in.
W	weight of pod	lb.
W_m	maximum value of W_r or W_s	lb/in.
W_r	longitudinal force per inch of circumference in ring	lb/in.
W_s	Longitudinal force per inch of circumference in joint	lb/in.
X	distance along centerline of pod	in.
X_s	distance from center to neutral axis of joint	in.
x	distance from aft edge of lug to forward corner bolt	in.
$\bar{x}$	x distance from R_z point of action to centroid of bolt pattern	in.
x_1	vertical distance along shank of button	in.
x_1	vertical distance of hardback centroid from pod centerline	in.
x_2	vertical distance of longeron centroid from pod centerline	in.
Y	aerodynamic side force at geometric center, + to port	lb.
YM	aerodynamic yawing moment about geometric center, + nose to port	in-lb.

LIST OF SYMBOLS (Continued)

Symbol	Meaning	Units
Y_r	vertical distance of point above bottom	in.
Y	distance of point on pod from neutral axis	in.
y'	distance from left edge of lug to a right corner bolt	in.
$\bar{y}$	y distance from R_z point of action to centroid of bolt pattern	in.
$\bar{Z}$	vertical distance of R_y above pod surface	in.
$\bar{Z}_2$	vertical distance of R_x above pod surface	in.
θ	direction of principal strain	
μ	Poisson's ratio	—
ϕ	angular location of a point on pod skin	deg

SUMMARY

External loads for the QRC-335A mounted on the F-4C (or RF-4C), F-105, and F-111 aircraft are used for this stress analysis From these loads. 18 distinct load conditions exist as follows:

Load Conditions 1 to 6 are flight loads on the F-4C, F-105, and F-111 pylons per reference 3.

Load condition 7 is a jettison load for worst case of F-4, F-105, or F-111 pylon per reference 3.

Load Condition 8 is the jettison load from the Sparrow Launcher in the missile well of the F-4C.

Load Condition 9 to 14 are flight loads on the RF-4C inboard pylon derived from McDonnell data on the QRC-160-8.

Load Conditions 15 to 18 are flight loads in the F-4C missile well derived from Sparrow loads.

For each load condition. one or more mounting configurations are involved. Each mounting configuration represents a particular suspension lug and particular geometric dimensions. Each mounting configuration is lettered to avoid confusion with load conditions. The combination of one mounting configuration with one load condition forms a load case. For example case B 3 is type B mounting configuration with load condition 3. There are a total of 30 applicable cases.

Because each load condition is comprised of 11 components (6 aerodynamic plus 5 inertial) and a mounting configuration is comprised of several different pieces of hardware and a number of dimensions it is generally true that one load case is critical at one location on the pod and other load cases are critical at other locations on the pod. Therefore all load cases have been considered at each possible critical location.

There are three general types of structural failure possible on this pod. They are:

1) failure of the suspension lug or its attaching screws.

2) failure of the V-band clamps, the clamp rings, or their attachment to the monocoque shell.

3) failure of the monocoque shell.

A computer routine was used to calculate the margin of safety for each of these types of failures for every possible failure location and for each load case. The resulting critical margins of safety (those less than 0.6) are listed in tables I and II.

Table I lists the critical margins for all load conditions with the pod on pylons. Only the QRC-335A with a ram air turbine generator was considered, because the loads are considerably less when the QRC-335A is flown without the generator. Because the QRC-335A uses a structure that was designed for longer pods, the margins of safety for all pylon load cases other than G-7 (jettison) are greater than 0.6 and thus do not appear in the table I. The jettison load causes fairly low margins, because the relatively low weight of the QRC-335A makes the acceleration due to the fixed jettison force very high. All of the critical stresses in table I are at the clamp rings or their attachment to the shell.

Table II lists the critical margins for all load conditions with the QRC-335A mounted in the F-4C missile well. In these cases, there is no ram air turbine generator because there is insufficient clearance for the turbine blades. In these conditions only load case E 17 caused margins less than 0.6. All of the critical margins in table II are at the forward lug (called button) or its attaching screws.

TABLE I

CRITICAL MARGINS OF SAFETY FOR QRC335 +GEN.

CONDITION	TYPE	LOCATION		M.S.
G 7	MSY	25	BEAR.	-.013
G 7	MSYT	25	BEAR.	-.043
G 7	MSUT	25	BEAR.	.566
G 7	MSY	26	SHEAR	.442
G 7	MSYT	26	SHEAR	.398
G 7	MSU	26	SHEAR	.442
G 7	MSUT	26	SHEAR	.398
G 7	MSY	26	BEAR.	-.173
G 7	MSYT	26	BEAR.	-.198
G 7	MSU	26	BEAR.	.410
G 7	MSUT	26	BEAR.	.311
G 7	MSY	29	SHEAR	.268
G 7	MSYT	29	SHEAR	.230
G 7	MSU	29	SHEAR	.268
G 7	MSUT	29	SHEAR	.230
G 7	MSY	30	A.RING	.495
G 7	MSYT	30	A.RING	.405
G 7	MSU	30	A.RING	.598
G 7	MSUT	30	A.RING	.502
G 7	MSY	31	SHEAR	.014
G 7	MSYT	31	SHEAR	-.017
G 7	MSU	31	SHEAR	.014
G 7	MSUT	31	SHEAR	-.017
G 7	MSY	31	BEAR.	.005
G 7	MSYT	31	BEAR.	-.026
G 7	MSUT	31	BEAR.	.566

Note: 1. Critical margins of safety are considered here to be those less than 0.600.

2. No margins of safety appear for flight loads because they are all higher than 0.600.

3. All negative margins of safety in above table are not significant since they are for jettison, where yielding is allowed.

TABLE II

CRITICAL MARGINS OF SAFETY FOR QRC335 'WELL

CONDITION	TYPE	LOCATION	M.S.
E17	MSY	41 BUT.A.	.002
E17	MSYT	41 BUT.A.	-.028
E17	MSU	41 BUT.A.	.054
E17	MSUT	41 BUT.A.	.023
E17	MSY	41 F.LUG	.477
E17	MSYT	41 F.LUG	.433
E17	MSU	43 F.L.SC	.365
E17	MSUT	43 F.L.SC	.324

1. Critical margins of safety here are considered to be those less than 0.600.

The meaning of "TYPE" in these tables is as follows:

MSY is a margin of safety calculated to check that yielding does not occur at limit load using a factor of safety of 1.15.

MSU is a margin of safety calculated to check that rupture does not occur at ultimate load (1.5 times limit load except for jettison where ultimate load was taken as 1.15 times the load based on actual jettison force.)

MSYT and MSUT are the same as MSY and MSU respectively but using material properties after exposure to 250° F for 10,000 hours.

As explained in the footnote to table I, yielding during jettison is immaterial, so all entries of MSY or MSYT in Table I can be ignored. Therefore, the only pertinent negative margins are rivet shear at location 31 for case G 7 where MSUT = - .017 and the button stress for case E 17 where MSYT = - .028. Because all assumptions through-out this analysis are conservative, these margins of safety are considered acceptable.

SECTION I

INTRODUCTION

1.1 PURPOSE AND SCOPE OF REPORT

This report is being submitted in accordance with the requirements of Air Force Contract No. F33657-67-C-0994. It consists of a load and stress analysis of the primary structure of the QRC-335A pod for carriage on the MAU-12 B/A bomb rack and on the Sparrow launcher. The pod configuration includes a RATG (ram-air turbine generator) for carriage on the bomb rack, but excludes the RATG for carriage on the Sparrow launcher. The loads are derived from loads on similar stores carried on the F-4C aircraft at the forward fuselage missile station and at the inboard wing pylon. In addition, the strength of the pod for carriage on any other aircraft is considered by analyzing it for "integration loads," which are severe load conditions representing critical loads on various high-performance aircraft. The resulting margins of safety are tabulated for all of the load conditions, for strengths at room temperature and elevated temperature (250° F exposure for 10,000 hours).

1.2 BACKGROUND-PREVIOUS ANALYSES

The structure of the QRC-335A pod is very similar to that used on various ECM pods made previously including the multi-purpose 669A pod, QRC-249A, and QRC-272 (T). The principal module (see figure 1 for identification of modules) is the same, except that the forward ring attachment has additional rivets and a gondola radome has been added. Since this section carries the lug and sway-brace reactions and the highest bending moments, it is the major structural member. Extensive tests and analysis using photoelastic coatings and strain gages have been done on the principal modules of other ECM pods; the data is summarized in reference 1. Results of these analyses are used in this report. Other major changes are the use of a casting to replace the wrap-around skin, longeron, and one end ring of the previous service-module riveted assembly; also, the forward end of the heat sink is attached to the service module instead of the principal module. A detailed description of the structure is given in Section I and the stress analysis methods are given in Sections III, IV, and V.

1.3 REVISIONS

1.3.1 REVISION A

The original report contained several errors, the major one being a sign error in the equations translating the load coordinate system for the Sparrow-derived loads which invalidated all subsequent results based on that data (all data on the E cases). This revision corrects the errors and contains supplementary explanations of the methods used for the load analysis.

1.3.2 REVISION B

Since the last publication of this report, an ECP has authorized several additional equipments to the pod. Furthermore, some preliminary vibration tests have been made as a proof test of the primary structure. Revision B accounts for the effects of the additional equipments on the stress analysis and incorporates the results of the vibration tests. The equipments added by the ECP are:

* O.S. Generator
* Oscillator
* Ramp Generator
* Three boards and 4 packages in printed circuit rack
* Delay Power Supply
* Door in adapter

The original weight allowance for the heat sink assembly was generous enough so that with these additional items its actual weight still falls within the 135.5

pounds of the original estimate. Therefore, no revision to the load analysis is necessitated. The door in the adapter is nonstructural and this was also anticipated in the original stress analysis so that no change to the analysis is required for this item. Therefore, this revision does not change any of the previous results but merely incorporates the vibration test results in Section VIII which is a new section.

1.3.3 Revision C The entire report has been rearranged to show each type of analysis completely in its own section. The method for computing joint capabilities has been included. Sample calculations have been included in each section for added clarity. Other minor corrections have been made throughout the report.

1.4 STRUCTURAL DESCRIPTION AND FEATURES

1.4.1 Configuration With RATG (Pylon Mounted)

The pod shown in figure 1 is composed of five individual sections or modules: a nose module, utility module (RATG), adapter, principal module, and tail module. Adjacent modules are joined by V-band clamps. The pod is mounted on the aircraft by two lugs which engage the hooks of the aircraft's suspension rack. The sway braces of the rack bear against the upper sides of the principal module to resist side loads. To mate with some racks, sway brace pads are attached to the pod since the sway brace bolts were not designed for an external store with a diameter as small as 10 inches. For the standard lugs, hole patterns have been provided in the hardback of the principal module to allow lug locations at 2-inch intervals.

Each V-band clamp is made of two semicircular halves joined by four bolts. The clamp is machined from a forged ring of 17-4 PH stainless steel, and the inner surfaces of the V-groove are coated with a dry lubricant.

The mounting lugs are machined from a forging of 4340 steel. The forging

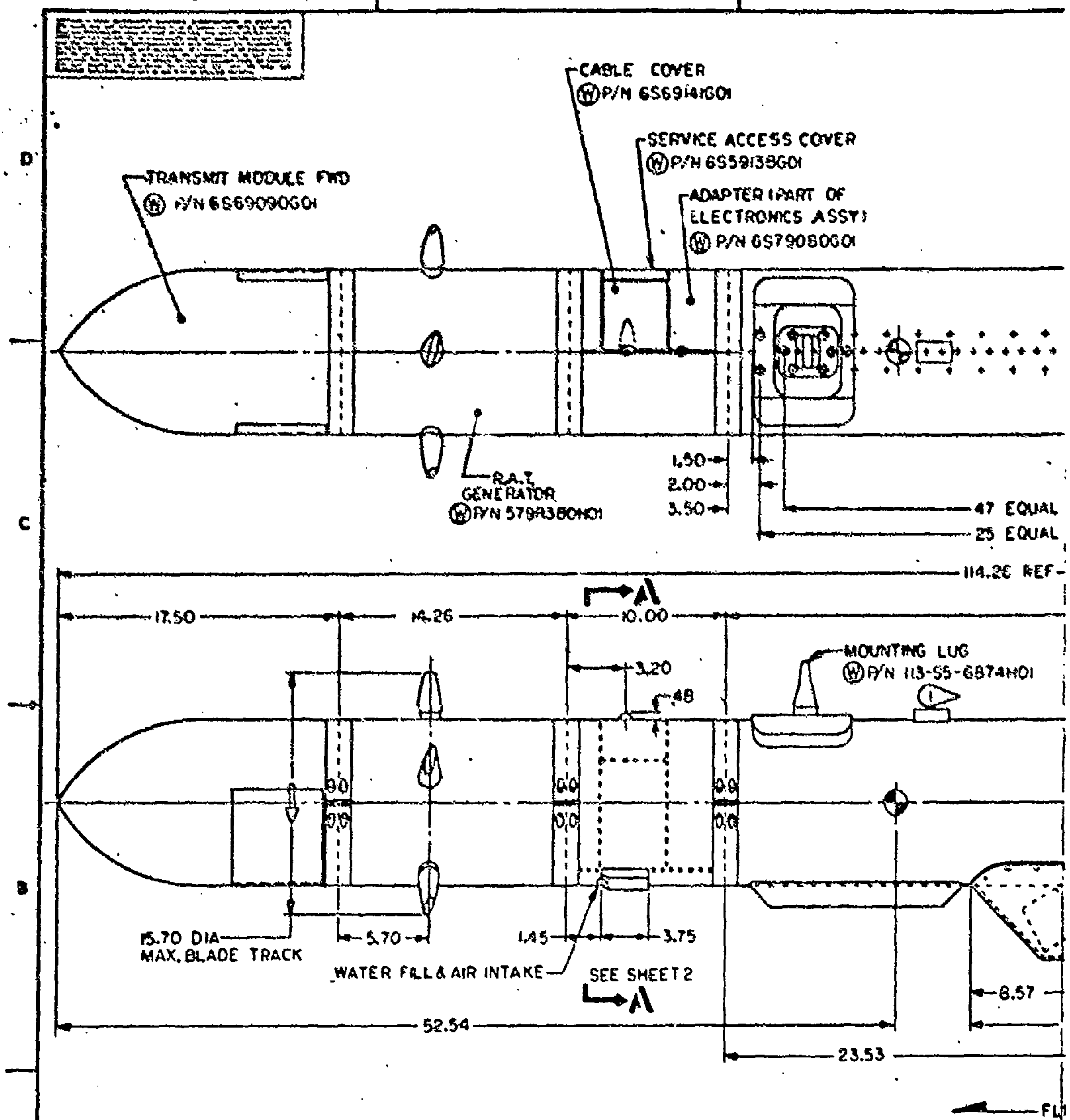

② INERTIA PARAMETERS OF POD (WITHOUT BALLAST AND MOUNTING HARDWARE) ARE:

WEIGHT = 307LB

MOMENTS OF INERTIA ABOUT C.G.

PITCH = 46.2 SLUG FT^2

YAW = 46.2 SLUG FT^2

ROLL = 1.1 SLUG FT^2

① SEE INSTALLATION KIT DWG 6S59100 FOR MOUNTING HARDWARE AND SEE "INSTALLATION DATA" FOR DETERMINING C.G. AND FOR POSITIONING MOUNTING HARDWARE is then heat-treated and cadmium-plated.

The sway brace pads are machined from aluminum and given a hard anodize finish.

1.4.2 Configuration Without RATG (Missile Well Installation)

The pod shown in figure 2 is of the same configuration, but has no RATG. The pod is to be used in this configuration (except for mounting hardware) wherever aircraft electrical power is available. The pod is expected to be used initially in this configuration on the Aero 27 centerline rack of the F-4C and on the Sparrow launcher in the forward fuselage of the F-4C. Lack of blade clearance precludes the use of the generator at these locations.

For installation on the Sparrow laucher, the convential lugs are replaced by a button forward and a hook aft as shown in figure 2. A special sway brace pad is used at the forward braces. The aft sway-brace pad is part of the hook. This suspension hardware is attached to the pod in the same manner at the standard lugs. The button and hook are made of AISI 4340 alloy steel.

1.4.3 Internal Features

All of the sections have a semimonocoque structure. For reinforcement the principal module has an internal hardback at the top to withstand lug and sway-brace reactions and a longeron at the bottom to withstand cradling loads. The hardback and longeron provide additional stiffness and strength for bending in the vertical plane and also function as slide rails for the electronic chassis. The hardback and longeron are fastened to the inside of the skin by countersunk screws, and this assembly is attached by a bolted and riveted lap joint to the end rings which engage the V-band clamps.

The end rings serve to maintain the roundness of the pod cross section, to facilitate mating with the V-band couplings, and to support the aft end of the chasis. The skin in conjunction with the circumferential stiffeners provides

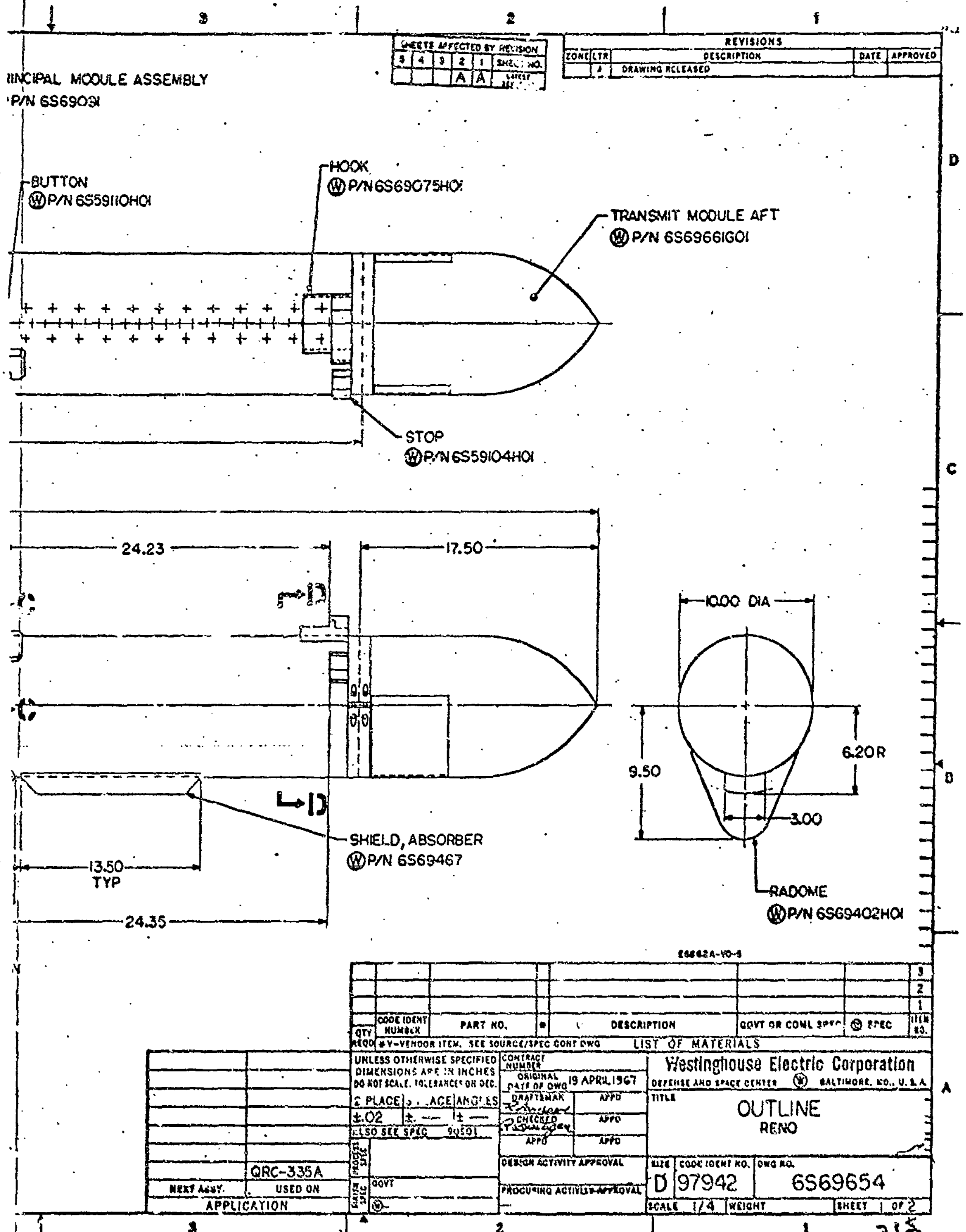

Figure 2. QRC-335A Pod Configuration for Mounting on Sparrow Launcher

beam strength to withstand the shear and bending moments in the horizontal and vertical planes. In addition, the skin provides environmental protection and gives an aerodynamic shape to the pod.

The skin of all sections except the radomes is 2024-T3 aluminum, 0.10-inch thick in the principal module and 0.125 -inch thick in adapter module. The end rings are machined from forged 17-4 PH stainless steel for heavily loaded joints and from 2024-T4 aluminum plate for lightly loaded joints. The hardback and longeron are machined from 2024-T4 aluminum bar stock.

The adapter module (figure 3) consists of a casting with the skin and an aft ring riveted to it. The skin is 2024-T3 aluminum and the ring is 17-4 PH steel. The casting consists of two heavy end rings joined by five longitudinal members and is made of A-356 aluminum alloy. The forward ring is machined to mate with the V-band clamp and is an integral part of the casting. On the right-hand side there is a nonstructural 150-degree cutout in the skin where there are two access doors. On the same side at the bottom is another nonstructural hinged cover which serves as a relief valve for excessive internal pressure. The forward end of the heat sink is bolted to the casting's top and bottom longitudinal members.

1.4.4 SUMMARY OF INERTIAL AND GEOMETRICAL Parameters

The inertial and geometrical parameters for the two pod configurations are given in Table III. These values are conservatively based on the maximum estimated weights of equipment; actual weights will probably be slightly less. Values are for pods with eight pounds of water in the heat sinks but without mounting hardware. (The mounting hardware depends on the particular installation.)

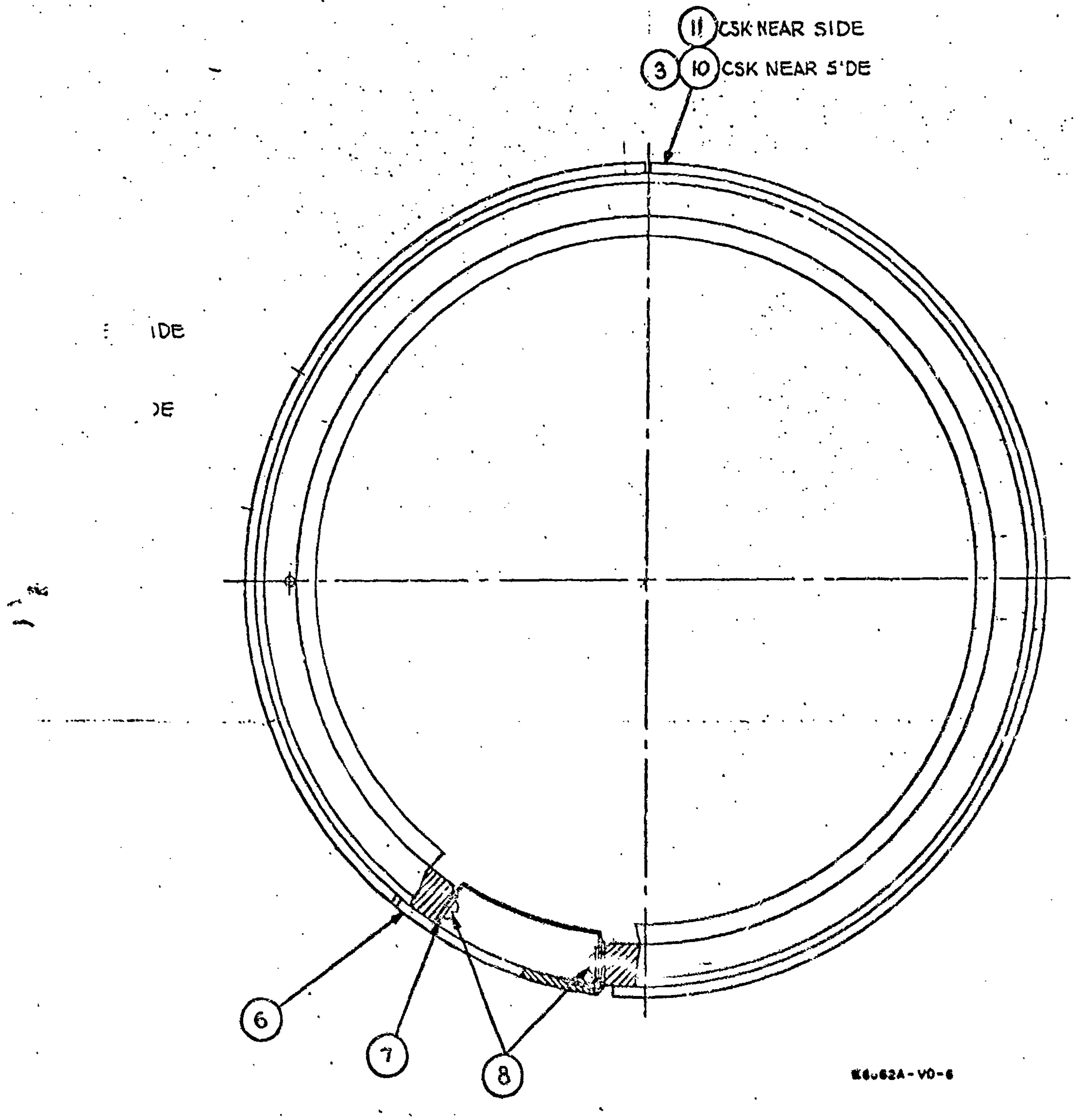

Figure 3. Adapter Module Structure

TABLE III

INERTIAL AND GEOMETRICAL PARAMETERS OF

QRC-335A POD

Parameter	Value With RATG	Value Without RATG
Length (in)	114.3	100.0
Diameter (in)	10	10
Weight (lb)	306.7	231.5
CG (station)	52.54	47.83
Pitching Mom. of Inertia ($lb-in^2$)	214,000	121,000

1.5 ANALYTICAL APPROACH

In section II the external loads that the pod must withstand will be determined. 18 distinct load conditions will be defined. Each load condition is composed of 11 components (three aerodynamic forces, three aerodynamic moments, three linear accelerations, and two angular accelerations). Because one component is largest for one condition and another component is largest for some different load condition, it is not obvious by inspection which load condition is most critical. Furthermore, one load condition may be critical at some location, such as the lugs, while a different load condition may be critical at another location such as the joints. Because of the large number of combinations of loads and possible failure locations, a computer routine has been used to calculate the margins of safety at each possible failure location for each load condition.

The possible failure locations divide into three general types, each with its own particular method of analysis. These three types of failures and their methods of analysis are described in the following paragraphs.

1.5.1 LUG STRESSES

The aerodynamic components of a load condition and the inertial components of a load condition are combined as described in MIL-A-8591 to form a net resultant load composed of three mutually perpendicular forces acting at the pod c.g. plus three mutually perpendicular moments acting at the pod c.g. Lug and sway brace reactions were calculated using the net resultant loads and the equations in MIL-A-8591. Each lug reaction is composed of three orthogonal components. By analysis or test (depending upon the lug) the strength of the lug to resist each of these components is known. The combined effect of the three components of the lug reaction has been calculated by using stress ratio. For instance, if a particular ultimate load causes a vertical lug force that is 50% of the vertical lug strength, plus a side lug forces that is 10% of the sidewards lug strength, plus a fore and aft lug force that is 10% of the axial lug strength, stress ratio indicates that the lug is stressed to 50 + 10 + 10= 70% of its capability, or that the margin of safety is 100% / 70% -1= 0.43. This is a conservative assumption, because the three components of the lug reaction will not all have maximum stress points that coincide.

Another margin of safety calculation that depends upon the lug reaction is the stress in the screws that attach the lugs to the pod. These screws are arranged around the lug in such a manner that there is always one corner screw that is put in tension by each of the components of the lug reaction. Axial and lateral forces load the screw by trying to tip the lug about the opposite edge. Therefore, the procedure is to find the maximum screw tension due to each component alone and to add all three maximum tensions to find the total maximum screw tension. This is compared to the actual screw strength to arrive at the margin of safety for the lug screws. Shear stress in the screws, caused by axial and lateral loads, can be neglected because it it relatively small and it is critical at a different location than the screw tension.

Lug and sway brace reactions and the resulting margins of safety for the lugs and lug screws are described in more detail in section III of this analysis. Sway brace reactions are included in section III for reference purposes only. Stresses in the pod structure caused by the concentrated lug and sway brace reactions are calculated directly from the external pod loads by a semi-empirical method that is described in paragraph 1.5.3.

1.5.2 Joint Stresses

The pod is composed of several sections or modules as shown in figures 1 and 2. The modules are held together by V-band clamps that engage a grooved ring on the end of each module. In general, each ring is a separate part that is riveted and/or screwed to the tubular module shell. Therefore, the internal bending moment at each joint could cause failure by any one of the following methods:

1) failure of the V-band clamp at its root
2) failure of either ring at its root
3) shearing of the rivets attaching either ring to its module
4) tearing of the skin of either module
5) bearing failure of either module skin at the rivets and/or screws.

The various rings are not identical. They are fabricated from different materials with different root thicknesses and different rivet spacings depending upon the design requirements of each location. Consequently, a generalized derivation has been used for calculating the margin of safety for these five possible failures at each joint. The generalized derivation is presented in appendix V.

The procedure for calculating the margins of safety at joints is as follows:

1) The vertical and horizontal component of the internal bending moment is calculated for each joint and for each load case.

2) Using the equations in appendix V and the appropriate material and geometric data, the moment capability of each joint is computed for both horizontal moments and vertical moments. Actually, both the moment that will cause yielding and the moment that will cause rupture are calculated.

3) The moment capabilities for yield and for rupture are compared with the actual moments due to limit and ultimate loads respectively to determine the margins of safety. The computer does this for all five possible methods of failure. Whichever produces the lowest margin of safety is obviously the actual failure mode for that joint.

The internal bending moments, the appropriate material and geometric data and the resulting margins of safety for the joints are presented in detail in section lV of this analysis.

1.5.3 Skin Stresses

The principal module of this pod has a relatively thick skin (0.100 inch) plus a curved hardback whose thickness varies with circumferential angle. As a result, the stress distribution caused by the concentrated loads at the lugs and sway braces is very complex. Attempts to calculate the pod strength by classical methods have predicted strengths in the order of 10% of that demonstrated in static tests. Therefore, an elaborate test was conducted, as described in reference 1, to establish a semi-empirical method for calculating the margin of safety of the skin stresses in the vicinity of the lugs and sway braces due to any combination of external loads.

The test consisted of mapping the skin stresses in a pod of the 669A type (the QRC-335A principal module structure is identical) by a photo-elastic technique. The ten most critical locations were found, and the stresses at each critical location were measured separately for measured magnitudes of:

1) positive vertical force
2) negative vertical force
3) positive pitching moment
4) negative pitching moment
5) positive side force
6) positive yawing moment

Both positive and negative vertical loads had to be measured, because the loading shifts from lugs to sway braces or vice versa. For side loads and yawing moment, no negative magnitudes were required, because there is symmetry with respect to these loads. Axial loads and rolling moments were not tested because they were very small for 669A pods. However, their principal effect has been included in the skin calculations by finding the equivalent pitching moment or side force respectively, where equivalent means that load which would produce the same sway brace reactions.

From the test data, coefficients were calculated for the shear stress, the circumferential bending stress at the outside of the skin, and the circumferential bending stress at the inside of the skin for each load component and for each of the ten critical locations. The load components consist of the six forces and moments listed above plus the symmetrical values for negative side force and for negative yawing moment. Thus, for each location, there are 24 coefficients, each of which is the magnitude of one of the three stresses caused by a unit force or a unit moment.

These coefficients are used to compute margins of safety for the skin stresses by the methods defined in appendix VI. Basically, it consists of determining the eight load components for each load case. Four of these components will be zero. For instance, if there is a positive vertical force, then the negative vertical force is treated as zero. Each component times the corresponding coefficient for a particular critical location gives a stress at that location due to that component. All stresses of the same type (for a given location) are algebraically added to give the total shear stress, the total outside bending stress, and the total inside bending stress. Max shear stress failure theory is then used to compute a resultant outside stress and a resultant inside stress. These are compared with the material strength to calculate the margins of safety.

1.6 DEFINITION OF CRITICAL LOCATIONS

Although there are only three general types of possible failure, each type could occur at a number of locations. Consequently, there are quite a few critical locations as shown in figure 4. As will be further defined in the next section, there are several possible configurations of the QRC-335A depending upon what aircraft is carrying it and where it is located on the aircraft. Figure 4 shows the two most important configurations and all others represent only minor modifications of these two configurations.

The following system is used in identifying critical points.

Points 11 to 20 are critical skin stress locations

Points 23 to 40 are joint stress locations

Points 41 to 44 are lug and lug screw locations.

Regardless of the configuration, a point number always has the same meaning. For instance, point 31 always means the forward ring on the principal module, and point 43 always means the screws that attach the forward lug. For different configurations, the actual location of a particular point number may change.

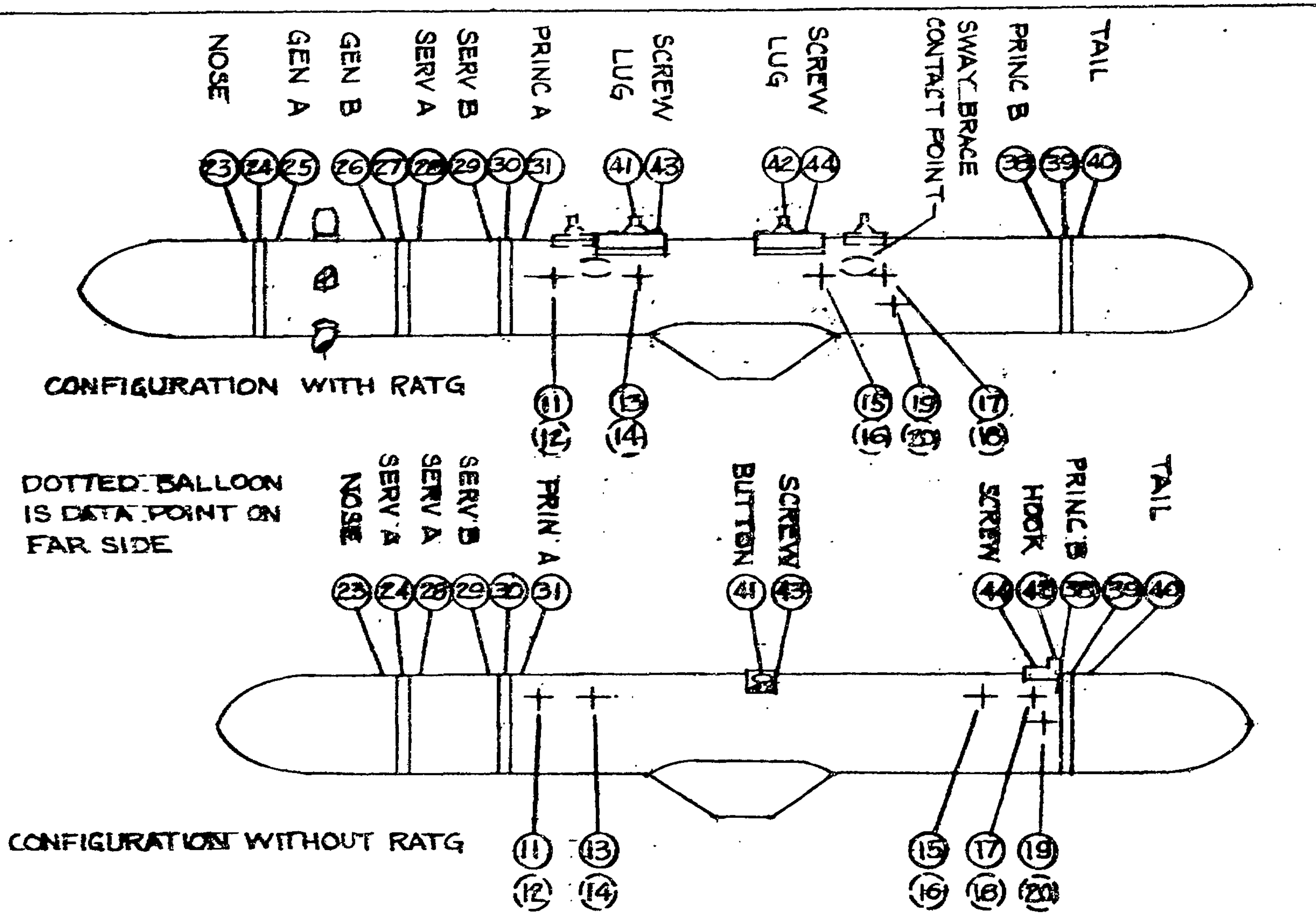

Figure 4. Location of critical points

Therefore, whenever possible, tables of results will indicate both the point number and its station. The station number is the distance in inches of the particular point from the tip of the nose of the pod.

SECTION II

EXTERNAL LOADS

2.1 AIRCRAFT AND MOUNTING RACKS

The QRC-335A pod can be carried at any of several locations on a variety of aircraft.

On the F-4C the pod would be used as follows.

A. If aircraft electrical power is available, a pod configuration similar to figure 2 (100 inch length and 231.5 pounds weight) could be carried at the following locations.

AERO 27 rack at centerline station.

Sparrow launcher at right forward missile well.

MAU-12 B/A rack at any pylon.

B. If aircraft electrical power is not available, a pod configuration with Ram Air Turbine Generator similar to figure 1 (114 inch length and 306.7 pounds weight) could be carried at the following locations.

MAU-12 B/A rack at any pylon.

The AERO-27 rack has mounting geometry very similar to that of the MAU-12 B/A. Loads for the shorter and lighter pod configuration without RATG will be less than those for the pod with RATG. Therefore, analysis for the pod with RATG on the MAU-12 B/A pylon will be sufficient for all cases except the Sparrow launcher which has completely different mounting geometry.

On the RF-4C the mounting locations are the same as on the F-4C except that the missile well location is not available. Aerodynamic loads and inertial loads on the RF-4C are identical to those on the F-4C, so no additional analysis is needed for the RF-4C.

On the F-105B the pod can only be carried on the wing pylons. These pylons have a Republic rack with 14 inch mounting centers. For this analysis it is assumed that the mounting geometry is equivalent to that of the MAU-12 B/A using 14 inch mounting centers. Because the F-105 loads are low compared with those for the F-4C and the F-111, the minor differences in sway brace locations are not critical.

On the F-111A the pod can be carried on any of the pivoted pylons. Normally, pylons number 3 and 6 are wired for ECM pods. These pylons have MAU-12 B/A racks.

2.2 EXTERNAL LOAD CONDITIONS

The 18 load conditions listed in table IV are the critical load conditions for the various aircraft and locations on the aircraft. These loads have been derived from the following sources.

Load Conditions 1 to 7 - "Integration loads" for 669A pods from reference 3. These are six of the most critical flight loads for pods on pylons on the F-4C, F-105B and F-111A aircraft plus the most severe jettison load on these aircraft. These are the same loads as those analyzed in reference 1, except that the length of the QRC 335A with RATG (114 inches) causes it to be in the intermediate length (100 to 130 inches). Reference 3 lists the aerodynamic and inertial loads for these seven conditions for short, intermediate and long pods of the 669A type. The data for load conditions 1 to 7 was taken directly from this source without modifications.

Load Condition 8 - Jettison from sparrow launcher. Data for this load condition was derived from the impulse curve supplied by McDonnell Aircraft Co. The impulse curve is shown in figure 11 in appendix III.

Load Conditions 9 to 14 - Flight loads with pod on inboard pylon of RF-4C aircraft based on McDonnell data for QRC-160-8. These loads have been

TABLE IV

DESCRIPTION OF LOAD CONDITIONS AND AIRCRAFT MANEUVERS

Load Condition	Aircraft Maneuver
1	Loads at station 189 on F-111A for case 2, figure 7 of MIL-A-8591 (reference 3)
2	Loads at station 189 on F-111A for case 6, figure 7 of MIL-A-8591 (reference 3)
3	Loads at station 189 on F-111A for case 3, figure 7 of MIL-A-8591 (reference 3)
4	Loads at station 132.5 on F-4C for symmetrical pullout: M=1.57, altitude = 20,000 ft, n_z = 6.5, p = 0, $\dot{p}$ = 0 (reference 3)
5	Loads at station 132.5 on F-4C for steady negative roll: M=0.8, altitude = 20,000 ft, n_z = 5.7, p = 267 deg/sec, $\dot{p}$ = 0 (reference 3)
6	Loads at station 170 on F-105B for symmetrical pushover: M=1.7, altitude = 35,000 ft (reference 3)
7	Jettison load
8	Loads due to jettison from Sparrow launcher semisubmerged in F-4C fuselage
9	Loads at station 81.50 RF-4C for symmetrical pushover: M=1.6, altitude = 20,000 ft, N_z = -3.0, p = 0, $\dot{p}$ = 0
10	Loads at station 81.50 on RF-4C for steady positive roll: M=0.8, altitude = 10,000 ft, N_z = 4.8, p = 200 deg/sec, $\dot{p}$ = 0
11	Loads at station 81.5 on RF-4C for symmetrical pushover: M=1.13, altitude = 0, N_z = -3.0, p = 0, $\dot{p}$ = 0
12	Loads at station 81.5 on RF-4C for symmetrical pushover: M=1.68, altitude = 20,000 ft, N_z = -3.0, p = 0, $\dot{p}$ = 0
13	Loads at station 81.5 on RF-4C for steady positive roll: M=1.68, altitude = 20,000 ft, N_z = 4.8, p = 69 deg/sec, $\dot{p}$ = 0
14	Loads at station 81.5 on RF-4C for steady positive roll: M=1.6, altitude = 20,000 ft, N_z = 4.8, p = 75 deg/sec, $\dot{p}$ = 0
15	Loads at Sparrow launcher semisubmerged in F-4C fuselage for symmetrical pullout: M = 0.64, N_z = 8.5, altitude = 0, p = 0, $\dot{p}$ = 0

TABLE IV (Continued)

Load Condition	Aircraft Maneuver
16	Loads at Sparrow launcher semisubmerged in F-4C fuselage for symmetrical pushover: $M = 1.92$, altitude = 40,000 ft, $N_z = 3.0$, $p = 0$, $\dot{p} = 0$
17	Loads at Sparrow launcher semisubmerged in F-4C fuselage for steady positive roll: $M = 0.76$, altitude = 10,000 ft, $N_z = 6.6$, $p = 260$ deg/sec, $\dot{p} = 0$
18	Loads at Sparrow launcher semisubmerged in F-4C fuselage for steady positive roll: $M = 1.82$, altitude = 40,000 ft, $N_z = -1.0$, $p = 114$ deg/sec, $\dot{p} = 0$

Note: Load factor, N_z, is at aircraft CG.

included in case the rolling moment due to the receive antenna radome causes loads more critical than the "integration loads" which did not include a rolling moment. Use of the QRC-160 data in appendix II requires scaling changes as described in section 2.4.

Load Conditions 15 to 18 - Flight loads with pod in missile well of F-4C aircraft based on McDonnell data for Sparrow missile. These loads have been included because the semi-submerged location plus extremely different mounting, makes these load conditions differ completely from installations on pylons. Use of the Sparrow data in appendix III requires scaling changes plus a rotation of reference axes as described in section 2.5.

The aerodynamic forces and moments and the inertial load factors for those load conditions that apply to wing pylons are given in table V. The entries for the first seven load conditions are directly from reference 3, and the entries for the last six load conditions are derived from the data in appendix II per the equations in section 2.4.

The aerodynamic forces and moments and the inertial load factor for those load conditions that apply to the F-4C missile well installation are given in table VI. These loads are derived from the data in appendix III per the equations of section 2.5.

2.3 CONFIGURATIONS AND LOAD CASES

Each load condition has one or more mounting configurations associated with it. For instance, load conditions on pylons using the MAU-12 B/A must consider using either the 14 inch or the 30 inch hook spacing. These mounting configurations have been lettered for identification as shown in table VII. Each configuration has a definite pod weight associated with it: 231.5 pounds if

TABLE V

AERODYNAMIC LOADS -LIMIT LOADS- FOR QRC335 +GEN.

NO.	Q	S	L	PM	YN	RM
1	500.	3325.	-882.	81200.	18930.	0.
2	500.	3325.	-882.	81200.	18930.	0.
3	500.	-1453.	345.	-78500.	-4000.	0.
4	467.	1490.	-204.	-10660.	95300.	0.
5	83.	695.	343.	17800.	-19540.	0.
6	770.	-242.	-665.	-56100.	5440.	0.
7	0.	0.	0.	0.	0.	0.
9	577.	-292.	-1195.	-33000.	-6450.	-418.
10	125.	1842.	-750.	6680.	6030.	2693.
11	640.	-489.	-920.	-42400.	-15850.	-710.
12	616.	-282.	-1025.	-35100.	-3330.	-417.
13	616.	1715.	-268.	-35100.	3500.	2522.
14	577.	1578.	-239.	-33700.	3260.	2310.

LOAD FACTORS FOR QRC335 +GEN, -LIMIT LOADS

NO.	NX,	NY	NZ	NTHETA	NPSI	SFU
1	2.00	1.50	-11.50	6.00	.00	1.50
2	2.00	7.50	-6.00	6.00	.00	1.50
3	2.00	-1.50	6.50	-6.00	.00	1.50
4	.00	.00	-6.50	.00	.00	1.50
5	.00	8.55	-8.10	.00	.00	1.50
6	.80	.00	2.50	.00	.00	1.50
7	.00	.00	52.17	.00	.00	1.15
9	.00	.00	3.00	.00	.00	1.50
10	.00	1.64	-6.38	.00	.00	1.50
11	.00	.00	3.00	.00	.00	1.50
12	.00	.00	3.00	.00	.00	1.50
13	.00	-.58	-4.98	.00	.00	1.50
14	.00	-.54	-5.02	.00	.00	1.50

Note: All symbols are defined in the List of Symbols.
Load factors, n, are at pod CG.
Aerodynamic loads are at geometric center of pod.

TABLE VI

LOAD FACTORS FOR QRC335 'WELL -LIMIT LOADS

NO.	NX,	NY	NZ	NTHETA	NPSI	SFU
8	.00	.00	21.60	-294.00	.00	1.15
15	.00	5.13	-6.81	.00	.00	1.50
16	.00	-1.81	2.40	.00	.00	1.50
17	.00	4.97	-6.35	.00	.00	1.50
18	.00	-1.83	-.46	.00	.00	1.50

AERODYNAMIC LOADS -LIMIT LOADS- FOR QRC335 'WELL

NO.	D	S	L	PM	YN	RM
8	0.	0.	0.	0.	0.	0.
15	33.	-1302.	154.	5899.	25940.	-5467.
16	87.	465.	-318.	2305.	-12672.	1020.
17	27.	-2462.	-1330.	14752.	32792.	-15953.
18	100.	1413.	773.	-11922.	-24406.	9200.

TABLE VII

MOUNTING CONFIGURATIONS

Configuration	RATG	Aircraft	Rack	Lug	Accessories	Applied Load Conditions
A	Yes	Any	MAU-12[1] (14 in)	Small[2]	None	1 through 6
B	Yes	Any	MAU-12[1] (30 in)	Large[3]	Sway Brace Pad[4]	1 through 6
C	Yes	F-4C	MAU-12 (14 in)	Small[2]	None	9 through 14
D	Yes	F-4C	MAU-12 (30 in)	Large[3]	Sway Brace Pad[4]	9 through 14
E	No	F-4C	Sparrow Launcher	Button and Hook	None	15 through 18
F	No	F-4C	Sparrow Launcher	Button and Hook	None	8
G	Yes	Any	Any	Any		7

1. MAC Rack, Bomb Ejection
2. Westinghouse Lug, P/N 113-S6-4836
3. Westinghouse Lug, P/N 113-S5-6874
4. Westinghouse Sway Brace Pad, P/N 2-S6-3960

without RATG and 306.7 pounds if with RATG. Each configuration also has definite lug and sway brace parameters as will be indicated in later tables.

Each valid combination of a mounting configuration and a load condition forms a load case. Thus load case B3 is mounting condition B with load condition 3. There are 30 load cases that must be investigated. In general, all 30 load cases will have different lug reactions and stress distributions because of the differences in external loads and/or mounting dimensions.

2.4 DERIVATION OF LOADS BASED ON QRC-160-8 DATA

Load conditions 9 to 14 have been derived from the load data on the QRC-160-8 (appendix II) using the principles established in appendix 1 of reference 1, except that the effect of the receive antenna radome or gondola has been compared to the effect of the blade antennas of the QRC-160-8 to arrive at appropriate scaling factors. McDonnell's sign convention for loads is the same as that employed in this report when the pod is mounted on the left wing. The QRC-160-8 pod is 10 inches in diameter, 105 inches long, weighs 300 pounds, and has four "blades" projecting from the bottom as shown in Appendix II. The QRC-335A with the generator is 10 inches in diameter, 114 inches long, weighs 306.7 pounds, and has a gondola and some small absorber shields projecting from the bottom as shown in figure 1. To estimate the effect of these projected areas on airloads, the geometries are considered as follows. Primed variables refer to the QRC-160-8 and unprimed variables refer to the QRC-335A. All conversion equations have a factor of 2/3 to change the ultimate loads (given in appendix II) to limit loads.

2.4.1 Side-Area Effects on Load Equations

The side area of projections for the QRC-160-8 is:

$$A' = 2\ (1.4 \times 3.6 + 8.9 \times 4.4)\ 2 = 88.28 \text{ in}^2$$

The area moment below the pod centerline is

$$M' = 2\ (1.4 \times 3.6)\ (5 + 1.4/2) + 2\ (8.9 \times 4.4)\ (5 + 8.9/2) = 619.5 \text{ in}^3$$

The corresponding values for the QRC-335A neglecting the small shield absorbers and considering only the gondola is

$$A = 4.5\ (10) = 45 \text{ in}^2$$

The area moment below the pod centerline is:

$$M = 45\ (5 + 2) = 315 \text{ in}^3$$

Based on these values the following conclusions are made:

(1) Since the area of the QRC-160-8 projection is larger, it is conservative to neglect the difference for side airloads. Therefore, the side and normal airloads are given by

$$L = 2/3\ L' \times \text{Length Ratio} = 2/3\ L'\ (114/105)$$

$$S = 2/3\ S'\ (114/105)$$

(2) Since the first moment of area is approximately twice as large for the QRC-160-8 projections, it is reasonable to use ½ of the QRC-160-8 rolling moment for the QRC-335A.

(3) Since the projections for both pods are near the center, they will have little effect of yawing. Therefore, the yawing moment for the QRC-335A is given by:

$$YM = 2/3\ YM'\ (114/105)^{1.8}$$

The length ratio raised to the 1.8 power is the scaling method for moments used in appendix 1 of reference 1.

2.4.2 Frontal-Area Effects on Load Equations

The frontal area of the QRC-160-8 projection is given by

$$A' = 8.9\ (1.8) = 16 \text{ in}^2$$

The frontal area of the QRC-335A projection is given by

$$A = 4.5\ (7.0) = 32 \text{ in}^2$$

The frontal area for the basic 10-inch diameter is

$$A_1 = 78.5 \text{ in}^2$$

Therefore, the drag force on the QRC-335A given by

$$D = 2/3\ D' \left(\frac{78.5 + 32}{78.5 + 16} \right)$$

The effect of these projections on the pitching moment is estimated by considering the product of the aerodymanic pressure and the first moment of area of the projection. The area moment of the gondola is

$$32\ (5 + 2) = 224 \text{ in}^2$$

The area moment of the QRC-160-8 projections is

$$16\ (5 + 4.45) = 151 \text{ in}^2$$

For a drag force of 800 pounds, the additional negative pitching moment for the QRC-335A is

$$PM = \left(\frac{800}{78.5 + 16} \right) (224 - 151)$$

$$PM = 620 \text{ in-lb ultimate}$$

This is only about 1 percent of the maximum negative pitching moment (- 54,810 in-lb) on the QRC-160-8 so it can be neglected. Therefore, the pitching moment is given by

$$PM = 2/3\ PM' \ (114/105)^{1.8}$$

2.4.3 Example Using QRC-160-8 Data

Load condition 9 is derived from the first column of the load data in appendix II, load condition 10 is derived from the second column in appendix II, etc.

As an example, the loads for load condition 9 using the first column of McDonnell data are computed as follows:

$S = 2/3\ (-390)\ (114/105) = -282$ lb

$L = 2/3\ (-1650)\ (114/105) = -1194$ lb

$PM = 2/3\ (-42570)\ (114/105)^{1.8} = -32908$ in-lb

$YM = 2/3\ (-8350)\ (114/105)^{1.8} = -6455$ in-lb

$D = 2/3\ (740)\ (1.17) = 577$ lb

$NZ = 2/3\ (1350/300) = 3$ g's

$NY = 0$

$NX = 0$

$RM = 2/3\ (\frac{1}{2})\ (-1255) = -418$ in-lb

2.5 DERIVATION OF LOADS BASED ON SPARROW DATA

2.5.1 Load Condition 8, Missile Well Jettison

When the pod is carried in the missile well, the maximum jettison forces per the McDonnell data, figure 11 in appendix III are:

1100 lbs at forward ejector (14 inches in front of pod c.g.)

3600 lbs at aft ejector (30 inches behind pod c.g.)

The total vertical force is 4700 lbs, so the vertical acceleration is

$$N_x = \frac{4700}{231.5} = 20.3 \text{ g.}$$

The value of 21.6 g in table VI was based on an earlier weight estimate and is conservative. These two forces have a combined moment about the pod c.g. of

$$1100\ (14) - 3600\ (30) = 15400 - 108{,}000 = -92600 \text{ in.lbs.}$$

The pitching moment of inertia of this configuration is 121,000 lb in ^{2} or 314 lb. in.sec.^{2}. Therefore the angular acceleration will be

$$n_\theta = M/I = -92600/314 = -295 \text{ rad/sec}^2$$

2.5.2 Load Condition 15 to 18, Missile Well Flight Loads

Data for flight loads for the Sparrow III 6B missile installed in the forward fuselage of the F-4C was submitted to Westinghouse by the McDonnell

Company and is reproduced in appendix III of this report. The Westinghouse computer routine uses a sign connection per MIL-A-8591, but the McDonnell data uses a sign convention that is positive for outboard directions. The QRC-335A is to be carried in the right forward missile well, so it is necessary to reverse the signs of side forces, yawing moments and rolling moments in the McDonnell data to get it to correspond to MIL-A-8591. The computer routine is also based on using limit loads (plus appropriate safety factor) so the McDonnell data which is ultimate loads must be multiplied by 2/3. A further complication is introduced by the fact that the data must be rotated through an angle of 37° because the mounting is not symmetrical with respect to aircraft vertical. This rotation will be explained in the following section.

2.5.2.1 Missile Well Mounting Geometry

When mounted in the missile well, the QRC-335A has special adapters that make it equivalent to a Sparrow missile. Instead of a forward lug, there is a knob that is called the button. Instead of an aft lug, there is projection called the hook. Screws in the aircraft fuselage bear on the pod in a manner similar to sway braces and hereafter these screws will be called sway braces. A cross section at the forward sway braces, the button, and the hook/aft sway braces (same Station) are shown in figure 5.

It is desired to define loads that can be analyzed by the equations of MIL-A-8591. This requires that Z direction forces lie in a plane containing the lugs and the pod centerline. However, inspection of figure 5 shows that the plane through the pod centerline and parallel to the aircraft vertical plane contains neither the hook nor the button. Actually, both the hook and the button are at different angles from the vertical. As a consequence a new coordinate system will be defined for purposes of applying MIL-A-8591 equations. This new coordinate system will be rotated from aircraft vertical by an angle that is

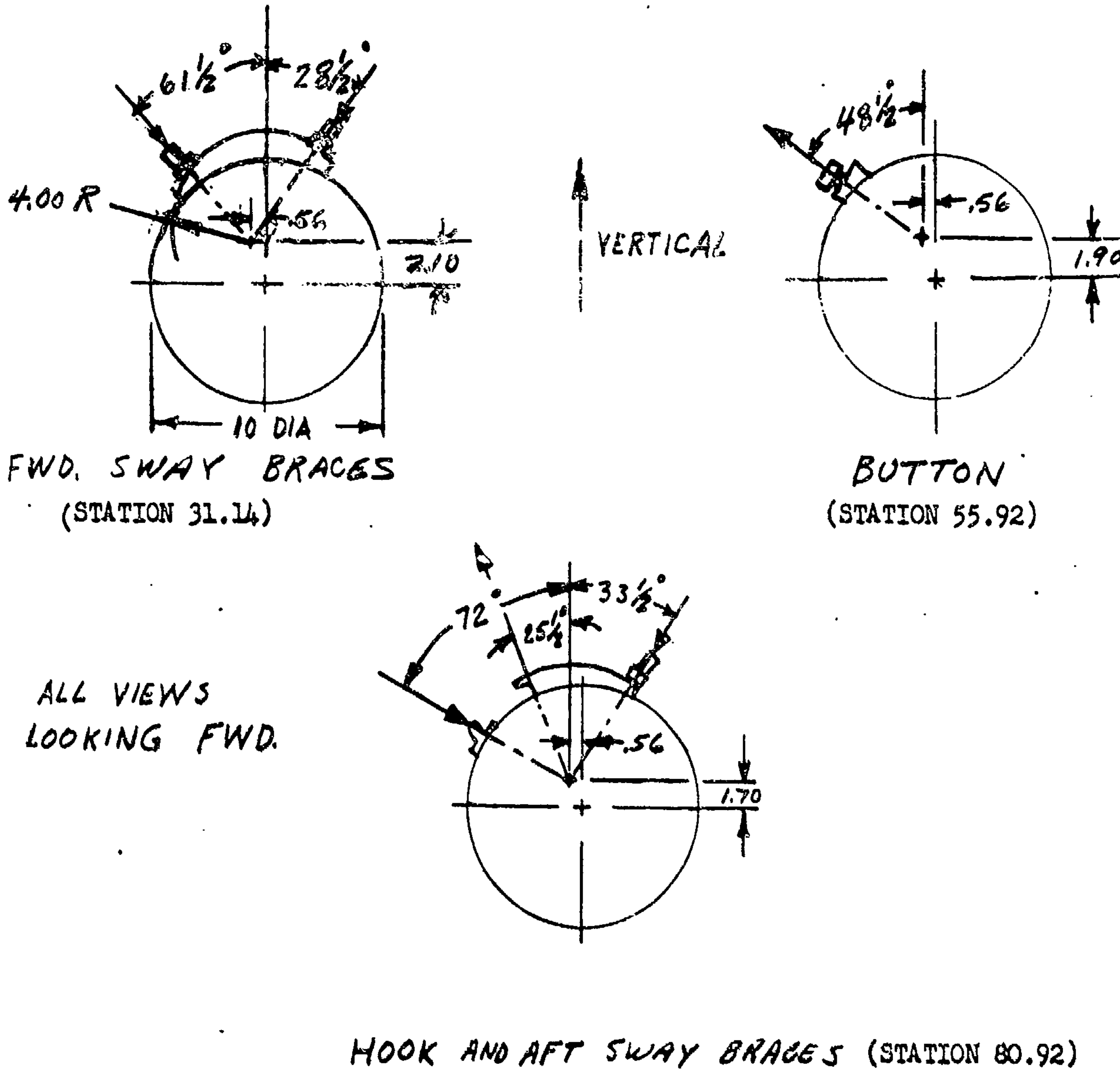

Note See figure 2 for plan and elevation views.

Figure 5 Geometry for Hook, Button, and Sway Braces half way between the angle of the button and the angle of the hook. Thus the angular rotation is

$$\theta = \frac{48.5 + 25.5}{2} = 37° \text{ CCW looking forward.}$$

The sway brace angles are not symmetrical as assumed in MIL-A-8591. Their angles in both the aircraft coordinate system and in the new coordinate system are listed in table VIII.

TABLE VIII
MISSILE WELL SWAY BRACE ANGLES

Position	Angle From Aircraft Vertical (Looking Fwd)	Angle From New direction (looking Fwd)	Median Angle New Coordinates
Left - Fwd	61.5 CCW	24.5 CCW	30 CCW
Left - Aft	72 CCW	35 CCW	
Right - Fwd.	28.5 CW	55.5 CW	58 CW
Right - Aft.	33.5 CW	60.5 CW	

To be conservative, the average of the left sway brace angles (in the new coordinate system) will be used for all sway brace when applying MIL-A-8591 equations.

2.5.2.2 Comparison of Configurations of QRC-335A and the Sparrow

The Sparrow has a large fin and its c.g. is aft of center. Its dimensions approximate 8 inches in diameter and 144 inches long. The QRC-335A has no fins, but it has a radome gondola near the center. Its c.g. is near center and it is 10 inches in diameter and 100 inches long. Because of the difficulty in extrapolating the Sparrow airloads to the QRC-335A, the airloads were assumed equal in both cases. Since the Sparrow is much longer and has large fin area, these airloads should be conservative for the QRC-335A. The inertial loads were assumed to be at the same g level as for the Sparrow, so they were obtained by dividing the given inertial load by the Sparrow weight of 455 pounds.

2.5.2.3 Equations for Converting Missile Well Load Data

The equations for obtaining the limit airloads from the McDonnell-furnished ultimate airloads are as follows, where the primed symbols refer to Sparrow data (aircraft coordinates) and the unprimed symbols refer to QRC-335A data (new coordinate system). The factor 2/3 accounts for the change from ultimate loads to limit loads. Reference to figure 6 will aid in seeing the origin of the signs and trigonometric functions. A similar diagram could be made for pitching and yawing moments or the equations can be derived from the equations for L and S by substituting PM for L and YM for S.

$$L = 2/3 \ (L' \cos\theta - S' \sin\theta)$$

$$S = 2/3 \ (-S' \cos\theta - L' \sin\theta)$$

$$PM = 2/3 \ (PM' \cos\theta - YM' \sin\theta)$$

$$YM = 2/3 \ (-YM' \cos\theta - PM' \sin\theta)$$

$$NZ = 2/3 \ (NZ' \cos\theta - NY' \sin\theta)$$

$$NY = 2/3 \ (-NY' \cos\theta - NZ' \sin\theta)$$

$$D = 2/3 \ (D')$$

$$RM = 2/3 \ (-RM')$$

2.5.2.4 Example

Load condition 15 corresponds to the first column of the McDonnell data, load condition 16 corresponds to the second column, etc.

As an example, the loads for load condition 15 are computed as follows:

$$S = 2/3 \ (-1420 \cos 37° - 1360 \sin 37°) = -1302 \text{ lb}$$

$$L = 2/3 \ (1360 \cos 37° - 1420 \sin 37°) = 154 \text{ lb}$$

$$PM = 2/3 \ (-16350 \cos 37° - (-36400) \sin 37°) = 5899 \text{ in-lb}$$

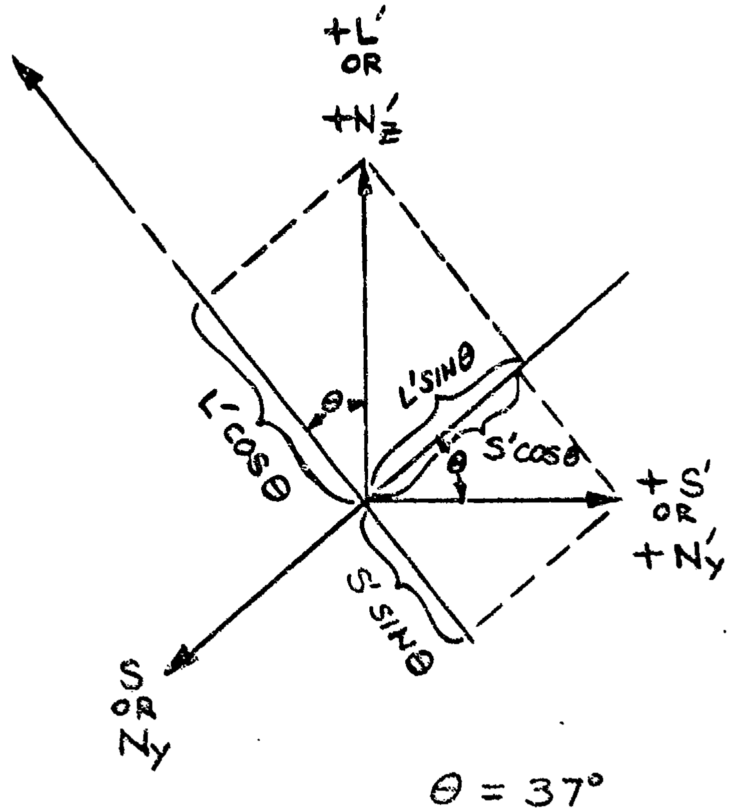

Figure 6 Rotation of Coordinate System

$$YM = 2/3 \left[-(-36400) \cos 37° - (-16350) \sin 37° \right] = 25940 \text{ in-lb}$$

$$D = 2/3 \left[50 \right] = 33 \text{ lb}$$

$$NZ = 2/3 \left[-5820/455 \cos 37° - 0 \right] = -6.81 \text{ g's}$$

$$NY = 2/3 \left[-0 - -5820/455 \sin 37° \right] = 5.13 \text{ g's}$$

$$RM = 2/3 \left[-8200 \right] = -5467 \text{ in-lb}$$

The converted data for all missile well flight loads are listed in table VI.

2.6 Net Resultant Loads

The aerodynamic loads and inertial load factors from tables V and VI have been combined in table IX to form the net resultant loads. Sign convention and equations for this combination are per MIL-A-8591. Thus

$$Px = D + W (Nx) \quad \text{etc.}$$

This table shows the net resultant load for each appliable load case (mounting configuration plus load condition) because these are the data that will be needed for further stress analysis. For missile well load cases, the coordinate system has been rotated as explained in section 2.5, so this data is appropriate for MIL-A-8591 type of analysis. Values of weight and moments of inertia for combining the inertial load factors are those given in table III.

For M y and M z there is an additional term because lift and side force are given at the pod center rather than at the c.g. Therefore,

$$M\,y = PM - (G-C.G.)\ L + I\ (N_Q)$$

$$M\,z = YM - (G-C.G)\ S + I\ (N_x)$$

TABLE IX

QRC335 +GEN. NET RESULTANT LIMIT LOADS

Load Case	PX	PY	PZ	MY	MZ	MX
A 1	1113	3785	-4408	88829	3436	0
A 2	1113	5625	-2721	88829	3436	0
A 3	1113	-1912	2339	-80626	2771	0
A 4	467	1490	-2199	-9699	88357	0
A 5	83	3317	-2140	16202	-22778	0
A 6	1015	-241	102	-53000	6568	0
B 1	1113	3785	-4408	88829	3436	0
B 2	1113	5625	-2721	88829	3436	0
B 3	1113	-1912	2339	-80626	2771	0
B 4	467	1490	-2199	-9699	88357	0
B 5	83	3317	-2140	16202	-22778	0
B 6	1015	-241	102	-53000	6568	0
C 9	577	-291	-274	-27430	-5088	-417
C10	125	2345	-2706	10175	-2553	2693
C11	640	-488	0	-38112	-13570	-709
C12	616	-281	-104	-30323	-2015	-416
C13	616	1537	-1794	-33850	-4491	2522
C14	577	1412	-1778	-32585	-4092	2310
D 9	577	-291	-274	-27430	-5088	-417
D10	125	2345	-2706	10175	-2553	2693
D11	640	-488	0	-38112	-13570	-709
D12	616	-281	-104	-30323	-2015	-416
D13	616	1537	-1794	-33850	-4491	2522
D14	577	1412	-1778	-32585	-4092	2310
G 7	0	0	16001	0	0	0

QRC335 +WELL NET RESULTANT LIMIT LOADS

Load Case	PX	PY	PZ	MY	MZ	MX
E15	33	-113	-1422	5565	28765	-5460
E16	87	46	238	2995	-13680	1020
E17	27	-1310	-2799	17638	38135	-15952
E18	100	989	667	-13598	-27471	9200
F 8	0	0	5000	-93958	0	0

Note: Resultant loads are at pod c.g.
Signs are per MIL-A-8591 C

SECTION III

LUG STRESSES

3.1 METHODS OF ANALYSIS

Lug and sway brace reactions were computed for all of the cases indicated in table IX using the equations in MIL-A-8591 (reference 2). Stress ratio was used to find the combined effect of the three components of the reaction at each lug. The combined stress ratio was then used to compute the margin of safety for each lug for all load cases. The lug reactions are also used compute the tension and margin of safety for the most heavily loaded lug attaching screw. Again, this is done for both lugs and for all loading cases.

3.2 Mounting Dimensions

The mounting dimensions needed for the MIL-A-8591 calculation are given in table X. The symbols are as similar as possible to the symbols in MIL-A-8591. The dimension H1 is not needed for lug reaction calculations, but it is needed later for calculating the maximum screw tension.

3.3 LUG AND SWAY BRACE REACTIONS

Lug and sway brace reactions were computed for all of the cases indicated in table IX using the equations in MIL-A-8591 (reference 2), except for the following modifications.

(1). Yawing moment was assumed to be reacted half by horizontal components of sway brace reactions and half by horizontal forces on the lugs. It is statically indeterminate how the yawing moment divides between the lugs and sway braces. The structure test program (reference 1) indicated that the half-and-half assumption is more realistic than the assumption in MIL-A-8591.

(2). Rolling moment, Mx, was added to the equations. It was assumed that the rolling moment divides between the two lugs in the ratio of

TABLE X
MOUNTING CONFIGURATIONS AND POD PARAMETERS

CONF.	LF	LA	LFB	LAB	BF	BA
A	-.22	14.22	2.78	17.22	35.00	35.00
B	-.22	30.22	-5.22	25.22	28.00	28.00
C	-.22	14.22	2.78	17.22	35.00	35.00
D	5.78	24.22	.78	19.22	28.00	28.00
G	1.30	1.70	1.30	1.70	.00	.00

CONF.	C	E	H	R	HI
A	1.70	-.19	1.40	5.00	.00
B	2.40	-2.39	2.10	7.80	.60
C	1.70	-.19	1.40	5.00	.00
D	2.40	-2.39	2.10	7.80	.60
G	.00	-.19	.00	5.00	.00

CONF.	LF	LA	LFB	LAB	BF	BA
E	-8.09	33.09	16.69	33.09	30.00	30.00
F	14.09	31.81	14.09	31.81	.00	.00

CONF.	C	E	H	R	HI
E	-.10	1.65	.94	4.00	.90
F	-.10	1.65	.94	4.00	.90

the lug distances from the C.G. in the same manner as side force divides between the lugs.

With respect to the option on dividing Px between the lugs, it was assumed that Px divides in the ratio of 2.1 between the more loaded lug and the less load lug respectively.

The lug and sway brace reactions for limit loads and for ultimate loads are given in tables XI and XII. As explained previously, for the missile well cases, configurations E and F, the forward lug refers to the button, and the aft lug refers to the hook. For missile well cases, the Z direction is 37° from aircraft vertical. Load case B2, an "integration load" for the F-111A, results in the highest lug and sway brace reaction for pylon installations. Load case E17 results in the highest lug and sway brace reactions for the missile well installation.

3.4 MARGINS OF SAFETY FOR LUGS

3.4.1 <u>Lugs for Bomb Racks</u>

The two lugs that are used on all racks except the Sparrow launcher are: a small lug (113-S6-4836) and a large lug (113-S6-2324). Stress ratio was used to determine the combined effect of axial, lateral, and vertical reactions on the lug. This implies that the ratio of the combined load maximum stress to the yield strength of the material is the summation of the ratios of each reaction component divided by the load in that direction that would cause yielding by itself. This is conservative because it assumes that the maximum stress point is coincident for all reaction components.

The lug strengths for the three directions are given in table XIII, where PSX, PSY, and PSZ are the loads, in the X, Y or Z direction that will cause the start of yielding. RUP is the lowest ratio of the load that will cause rupture

TABLE XI

WRC335 +GEN. LUG REACTIONS (LIMIT LOADS)

CONDITION	RFZ	RFX	RFY	RAZ	RAX	RAY	RFMAX	RFMIN	RAMAX	RAMIN
A 1	4154	371	-236	5500	742	124	5663	0	740	0
A 2	5031	371	-291	5487	742	125	8343	0	1173	0
A 3	5369	742	-40	0	371	98	2666	0	3657	3087
A 4	8519	311	-3200	1481	156	3156	6021	0	3501	0
A 5	4564	55	713	2175	28	-811	3839	0	1773	0
A 6	3467	677	-226	0	338	234	66	0	2317	1974
B 1	7841	742	-977	5110	371	64	7895	0	1779	0
B 2	9015	742	-1424	6245	371	67	11645	0	2555	0
B 3	3863	742	419	0	371	43	3750	0	1966	1307
B 4	8141	311	-1834	4602	156	1475	7746	0	5333	0
B 5	5747	55	-426	1456	28	-373	5546	0	186	0
B 6	2436	677	-50	0	338	109	143	0	1489	1241
C 9	2831	385	124	0	192	-180	745	0	1256	1119
C10	5861	83	448	696	42	-96	3936	0	765	0
C11	3904	427	387	0	213	-482	1470	0	1873	1423
C12	2701	411	14	0	205	-70	596	0	1289	1283
C13	6585	411	514	0	205	-165	2635	0	1932	1280
C14	6272	385	470	0	192	-150	2421	0	1832	1234
D 9	2062	385	108	0	192	-78	811	0	731	482
D10	4913	83	-194	1651	42	-98	4062	0	306	0
D11	2875	427	264	0	213	-216	1629	0	1157	471
D12	1932	411	55	0	205	-28	631	0	762	676
D13	4812	411	-18	0	205	-96	2669	0	552	195
D14	4584	385	-18	0	192	-88	2453	0	525	199
G 7	0	0	0	0	0	0	4533	4533	3467	3467

WRC335 WELL LUG REACTIONS (LIMIT LOADS)

CONDITION	RFZ	RFX	RFY	RAZ	RAX	RAY	RFMAX	RFMIN	RAMAX	RAMIN
E15	3555	0	-2090	46	33	946	1096	0	1422	0
E16	0	0	567	364	87	-344	161	80	454	0
E17	13100	0	-5616	0	27	1949	5655	0	5072	968
E18	6020	0	3452	0	100	-1256	3679	0	3366	663
F 8	0	0	0	0	0	0	709	709	1791	1791

TABLE XII

WRC335 +GEN. LUG REACTIONS (ULTIMATE LOADS)

CONDITION	RFZ	RFX	RFY	RAZ	RAX	RAY	RFMAX	RFMIN	RAMAX	RAMIN
A 1	6231	557	-354	8250	1113	187	8494	0	1110	0
A 2	7546	557	-437	8230	1113	188	12515	0	1760	0
A 3	8054	1113	-61	0	557	147	3998	0	5486	4630
A 4	12779	467	-4800	2221	233	4734	9032	0	5251	0
A 5	6845	83	1070	3262	41	-1217	5758	0	2659	0
A 6	5201	1015	-340	0	508	352	99	0	3475	2961
B 1	11762	1113	-1466	7665	557	96	11843	0	2669	0
B 2	13523	1113	-2137	9367	557	101	17467	0	3833	0
B 3	5794	1113	629	0	557	64	5626	0	2949	1960
B 4	13712	467	-2751	6904	233	2213	11612	0	8000	0
B 5	8620	83	-640	2184	41	-560	8319	0	279	0
B 6	3654	1015	-75	0	508	164	215	0	2234	1862
C 9	4247	577	186	0	288	-270	1118	0	1885	1679
C10	8792	125	672	1044	62	-144	5904	0	1147	0
C11	5856	640	580	0	320	-724	2205	0	2809	2134
C12	4051	616	21	0	308	-106	895	0	1934	1925
C13	9877	616	771	0	308	-248	3952	0	2899	1920
C14	9408	577	705	0	288	-226	3631	0	2747	1850
D 9	3092	577	161	0	288	-118	1216	0	1096	723
D10	7369	125	-291	2477	62	-148	6093	0	460	0
D11	4312	640	395	0	320	-325	2443	0	1735	706
D12	2898	616	82	0	308	-42	947	0	1143	1014
D13	7218	616	-28	0	308	-145	4004	0	829	293
D14	6876	577	-27	0	288	-132	3679	0	788	298
G 7	0	0	0	0	0	0	5214	5214	3987	3987

WRC335 +WELL LUG REACTIONS (ULTIMATE LOADS)

CONDITION	RFZ	RFX	RFY	RAZ	RAX	RAY	RFMAX	RFMIN	RAMAX	RAMIN
E15	5337	0	-3155	68	50	1419	1644	0	2133	0
E16	0	0	351	547	131	-517	241	120	682	0
E17	19650	0	-8424	0	41	2924	8780	0	7609	1452
E18	9041	0	5176	0	150	-1885	5518	0	5052	1024
F 8	0	0	0	0	0	0	616	616	2060	2060

TABLE XIII

LUG DATA FOR QRC335 .GEN.

CONF.	FORWARD LUG PSX	PSY	PSZ	RUP	MATERIAL	AFT LUG PSX	PSY	PSZ	RUP	MATERIAL
A	14000.	24000.	34000.	126	ALLOY	14000.	24000.	34000.	1.50	ALLOY
B	19100.	8760.	60000.	1.50	ALLOY	19100.	8760.	60000.	1.50	ALLOY
C	14000.	24000.	34000.	1.26	ALLOY	14000.	24000.	34000.	1.50	ALLOY
D	19100.	8760.	60000.	1.50	ALLOY	19100.	8760.	60000.	1.50	ALLOY
G	14000.	24000.	34000.	1.26	ALLOY	14000.	24000.	34000.	1.15	ALLOY

LUG DATA FOR QRC335 .WELL

CONF.	FORWARD LUG PSX	PSY	PSZ	RUP	MATERIAL	AFT LUG PSX	PSY	PSZ	RUP	MATERIAL
E	10000.	10680.	22250.	1.65	ALLOY	15500.	14600.	5270.	2.45	ALLOY
F	10000.	10680.	22250.	1.65	ALLOY	15500.	14600.	5270.	2.45	ALLOY
X	10000.	10680.	22250.	1.65	ALLOY	15500.	14600.	5270.	2.45	ALLOY

For the elevated temperature condition, these strengths are reduced to some percentage of the room temperature strengths above based on material properties in Appendix III to the load that will cause yielding. For configurations A,C, and G (where small lug is used), PSX and PSZ and RUP were determined by static tests. All other numbers in table XIII were calculated from the lug dimension. The large lug is very similar to the lug of figure 2 in MIL-A-8591.

For yield margin of safety, the total stress ratio is

$$FT_j = \frac{|R_{x_j}|}{PSX} + \frac{|R_{y_j}|}{PSY} + \frac{|R_{z_j}|}{PSZ}$$

where

R_{x_j} = limit load axial force on jth lug

R_{y_j} = limit load side force on jth lug

R_{z_j} = limit load vertical force on jth lug

The yield margin of safety then is

$$MSY = \frac{1}{SFY\ (FT_j)} - 1$$

where

SFY = yield safety factor = 1.15

For ultimate margin of safety the total stress ratio is

$$Ft_{ju} = \frac{|R_{x_{ju}}|}{RUP\ (PSX)} + \frac{|R_{y_{ju}}|}{RUP\ (PSY)} + \frac{|R_{z_j}|}{RUP\ (PSZ)} = 1.5\ \frac{Ft_j}{RUP}$$

where R_{xju}, R_{yju} and R_{zju} are ultimate load forces on jth lug.

The ultimate margin of safety is

$$MSU = \frac{1}{Ft_{ju}} - 1 = \frac{RUP}{1.5\ Ft_j} - 1$$

For margins after exposure to high temperature there is a derating factor, so,

$$MSYT = \frac{CTY}{SFY\ (FTj)} - 1$$

and

$$MSUT = \frac{RUP\ (CTY)}{1.5\ (FTj)} - 1$$

As an example, consider the forward lug point 41 in case B2.

$$FT = \left|\frac{742}{19100}\right| + \left|\frac{-1424}{8760}\right| + \left|\frac{9015}{60000}\right|$$

$$= .039 + .162 + .150 = .351$$

$$MSY = \frac{1}{1.15\ (.351)} - 1 = 2.48 - 1 = 1.48$$

$$MSU = \frac{1.5}{1.5\ (.351)} - 1 = 2.85-1 = 1.85$$

$$MSYT = \frac{.97}{1.5\ (.351)} - 1 = 2.40-1 = 1.40$$

$$MSUT = \frac{1.5\ (.97)}{1.5\ (.351)} - 1 = 2.76-1 = 1.76$$

Margins of safety for forward and aft lugs appear in summary tables as location or point number 41 and 42 respectively.

3.4.2 Lugs for Sparrow Launcher

The lugs for the missile well installation are: a button (Westinghouse No. 6-S5-9110) used as the forward lug and a hook (Westinghouse No. 6-S6-9075) used as the aft lug. The launcher is constructed in such a manner that only the hook can carry axial loads. Therefore RFX is zero in tables XI and XII for all missile well load cases. Because it is a critical design element, the button has been analyzed more exactly than the conventional lugs.

3.4.2.1 Button

The button used as the forward attachment for installation in the Sparrow missile well is shown in figure 7. It is machined from a 4340 steel plate, and is attached to the pod by six screws just as the lugs are.

The point of maximum stress in the Sparrow type button for combined vertical and lateral reactions is dependent on the ratio of the reaction. It is also dependent on the shape of the shank as it is broader at the base than it is at the top. If the vertical reaction predominates, a stress concentration factor of 1.5 should be used due to the abrupt change in cross section immediately under the head. The critical stress will be just under the head. If the lateral load predominates, the critical stress area will be further down the shank and the stress concentration factor therefore will not apply.

For these reasons, the margin of safety is computed at two points on the button: (41 BUT.A) on the shank where the stress is primarily caused by lateral forces, and (41F. LUG) just under the head where there is no bending but the stress concentration factor must be used.

By inspection of table XI, the worst case is E17 since both R_{yj} and R_{zj} are maximum. The maximum stress is determined by calculating the stress at various cross sections as follows:

$$f_t = \frac{P}{A} + \frac{Mc}{I}$$

$$f_t = \frac{Rz}{\pi r^2} + \frac{4Ry}{\pi r^3}$$

For E17

$R_z = 13100$ lb.

$R_y = -5616$ lb.

The contact force R_{yj} is displaced toward the bottom of the clevis due to deflection of the button and deformation of the clevis. If h is the length of the effective contact area, the effective force will be .22 - h/2 from the bottom of the head as shown in figure 7.

h is given by

$$F_{bry}\, d\, h = 1.15\,(Ry)$$

$$h = \frac{(1.15)(5616)}{(268000)(.500)}$$ (Fbry for 4340 is 268000 psi per Mil Handbook 5)

$h = .048$ inches

Thus the effective force Ry acts .20 from the bottom of the head.

Let x_1 be the distance measured along the shank from the point of application of R_y. Then a table can be constructed giving the stress as a function of x_1

x_1	r_1	πr_1^2	$4/\pi r_1^3$	Direct Stress (f_d) $\frac{R_z}{\pi r_1^2}$	Bending Stress (f_b) $\frac{4 x_1 R_y}{\pi r_1^3}$	Maximum Stress (f_t) $f_d + f_b$
.12	.25	.195	81.5	66,700	54,600	121,300
.16	.253	.201	78	65,900	71,400	137,300
.20	.258	.209	74	62,800	83,300	146,100
.22	.264	.217	71	60,600	86,800	147,400
.24	.269	.227	65	58,000	88,700	146,700
.28	.285	.255	55	51,900	87,400	139,300

The maximum stress occurs at $x_1 = .22$

From the table of Material Strengths, Table XXXIII:

$F_{ty} = 170,000$ psi

$F_{tu} = 188,000$ psi

The margin of safety for yielding at room temperature is

$$MSY = \frac{F_{ty}}{1.15\, f_t} - 1$$

$$MSY = \frac{170}{(1.15)(147,400)} - 1$$

MSY = .002

If perfect plastic behavior were attained in bending, the ultimate bending moment is given by

$$M_u = \left(\frac{16}{3\pi}\right)\left(\frac{F_{tu}}{F_{ty}}\right)\left(M_y\right)$$

$$M_u = \left(1.7\right)\left(F_{tu}/F_{ty}\right)\left(M_y\right)$$

Even though 4340 steel of this temper is tough (45% reduction of area for this temper for round specimens in tension), a reduced factor of 1.15 instead of 1.7 will be used to be conservative.

$$M_u = 1.5 \left(\frac{F_{tu}}{F_{ty}}\right) M_y$$

$$M_u = 1.5 \left(\frac{188}{170}\right) M_y$$

$$M_u = 1.65 \; M_y$$

This is equivalent to saying that the modulus of rupture, F_{bu}, is

$$F_{bu} = 1.5 \; F_{tu}$$

$$F_{bu} = 1.5 \; (188{,}000)$$

$$F_{bu} = 282{,}000 \text{ psi}$$

For combined tension and bending for ultimate loads, add the stress ratios:

$$R_{ult} = R_T + R_B$$

$$R_{ult} = \frac{1.5 \; f_d}{F_{tu}} + \frac{1.5 \; f_b}{F_{bu}}$$

$$R_{ult} = \frac{1.5 \; (60{,}600)}{188{,}000} + \frac{1.5 \; (86{,}800)}{282{,}000}$$

$$R_{ult} = .484 + .462$$

R_{ult} = .946

$\overline{MSU}$ = 1/R - 1

MSU = .054

Derating the strengths to 97% of room temperature strength for the higher service temperatures gives

MSYT = - .028

MSUT = .023

NOTE: All margins would be positive if the larger sway brace angles on the outboard side were included in the lug reaction calculations.

These margins are shown in table XIV as point 41 BUT.A. Table XIV, which shows all the margins of safety for the worst load case (E17), also shows that the margins at the stress concentration just under the button head (41F [illegible]) are much higher than at the critical location (41 BUT A).

3.4.2.2 Hook

The hook used as the aft attachment for installation in the Sparrow missile well is shown in Figure 8. This hook is made of the same material as the button, but has heavier sections and much lower loads, so the margins of safety are very high (600%+). Therefore a detailed analysis is not presented here. The strengths given in Table XIII were derived by an analysis similar to that of the button.

3.5 LUG FASTENERS

The lugs are attached to the hardback of the pod via high-strength screws and solid-wall inserts in the hardback. The inserts are weaker than the screws; thus, the margins of safety for pulling off the lugs are based on the insert strength. All of the inserts are of the same strength, except for one of a different type at the "B" end. This one is somewhat weaker so that an insert

TABLE XIV
MARGINS OF SAFETY FOR ALL DATA POINTS FOR CRITICAL CASE E17

POINT	X	FT	MSY	MSU	MSYT	MSUT
11 OUTS.	60.2	7270.99	7.434	9.586	6.422	7.469
11INSIDE	60.2	7340.93	7.353	9.485	6.351	7.388
12 OUTS.	60.2	15822.41	2.876	3.865	2.411	2.892
12INSIDE	60.2	15633.81	2.922	3.923	2.452	2.939
13 OUTS.	63.5	5569.10	10.011	12.821	8.690	10.057
13INSIDE	63.5	6092.98	9.064	11.633	7.857	9.106
14 OUTS.	63.5	18978.15	2.231	3.056	1.843	2.245
14INSIDE	63.5	19057.56	2.218	3.039	[illegible]	2.231
15 OUTS.	72.2	14576.85	3.207	4.280	2.702	3.224
15INSIDE	72.2	20824.89	1.945	2.696	1.591	1.957
16 OUTS.	72.2	11226.54	4.462	5.856	3.807	4.485
16INSIDE	72.2	16508.82	2.714	3.662	2.269	2.730
17 OUTS.	79.0	13708.14	3.473	4.615	2.937	3.492
17INSIDE	79.0	20159.86	2.042	2.818	1.677	2.054
18 OUTS.	79.0	15860.48	2.866	3.853	2.402	2.882
18INSIDE	79.0	20247.46	2.029	2.801	1.665	2.041
19 OUTS.	79.5	18188.46	2.371	3.232	1.967	2.385
19INSIDE	79.5	24793.68	1.473	2.104	1.176	1.484
20 OUTS.	79.5	12920.91	3.746	4.957	3.176	3.766
20INSIDE	79.5	16809.35	2.648	3.579	2.210	2.665
23 SHEAR	16.1	688.90	78.309	59.804	75.930	57.980
23 BEAR.	16.1	688.90	106.220	136.744	103.003	127.102
23 TEAR.	16.1	688.90	498.520	573.448	438.578	458.559
24F.RING	17.5	975.68	41.660	38.247	36.540	32.752
24V-BAND	17.5	975.68	450.517	369.036	423.426	346.834
24A.RING	17.5	975.68	198.340	206.409	184.386	171.149
28 SHEAR	18.9	1313.04	661.252	506.727	641.385	491.495
28 BEAR.	18.9	1313.04	661.252	506.727	641.365	471.186
28 TEAR.	18.9	1313.04	184.431	191.936	162.179	153.349
29 SHEAR	26.1	3845.35	31.182	23.673	30.216	22.932
29 BEAR.	26.1	3845.35	57.974	74.763	56.205	69.450
29 TEAR.	26.1	3845.35	206.244	237.331	181.375	189.605
30F.RING	27.5	4492.41	97.162	79.447	91.272	74.620
30V-BAND	27.5	4492.41	97.062	79.366	91.179	74.544
30A.RING	27.5	4492.41	34.445	28.049	32.319	26.306
31 SHEAR	28.9	5189.81	21.612	16.336	20.934	15.816
31 BEAR.	28.9	5189.81	21.414	27.795	20.742	25.780
31 TEAR.	28.9	5189.81	93.117	107.235	81.823	65.588
32 SHEAR	80.6	3901.88	67.790	51.739	65.726	50.157
32 BEAR.	80.6	3901.88	126.562	162.878	122.736	151.406
32 TEAR.	80.6	3901.88	100.303	115.498	88.147	92.199
39F.RING	82.5	2356.73	228.505	187.089	214.735	175.804
39V-BAND	82.5	2356.73	185.927	152.194	174.711	143.005
39A.RING	82.5	2356.73	16.661	15.248	14.542	12.975
40 SHEAR	83.9	1848.23	28.561	21.664	27.675	20.984
40 BEAR.	83.9	1848.23	38.965	50.342	37.766	46.746
40 TEAR.	83.9	1848.23	185.190	213.118	162.847	170.295
41BUT.A.	55.9	1.04	.002	.054	-.028	.023
41 F.LUG	55.9	.59	.477	.868	.433	.812
42 A.LUG	80.9	.14	5.429	11.075	5.236	10.713
43F.L.SC	55.9	4053.15	.781	.365	.727	.324
44A.L.SC	80.9	1268.29	4.691	3.363	4.520	3.232

strength value is used which conservatively averages both types.

For bolt tension induced by loads on large and small lugs assume:

1) Only 5 bolts are effective for direct vertical load because of non-uniform loading of bolts. This is substantiated by limited tests.

2) Angle of bolts from center of pattern (12° max.) is negligible so that Z' reaction loads induced at bolts are tension loads and X and Y' reaction loads are shear loads where Z is parallel to center bolts and Y is perpendicular to X and Z.

3) The moment about one edge of the lug due to external horizontal loads causes the lug to pivot about that edge (i.e. lug and hardback are rigid compared with elasticity of bolts). Therefore the bolt load is proportional to its distance from the pivoting edge. Also, preload does not add to induced bolt load so it is conservative to neglect preload.

Based on these assumptions the highest loaded bolt will always be a corner bolt. Note that the weakest element is the insert rather than the bolt even when the bolts are carrying the shear load induced by the maximum lateral and axial lug forces, so it is not necessary to consider bolt shear loads, since the margins of safety are based on insert pull-out.

For the hook, (the aft "lug" of the missile well installation), the reaction loads are at an angle Θ(measured clockwise looking aft) from the center of the bolt pattern. The "lug" reactions are given for the X,Y,Z coordinate system so that the components in the X,Y',Z' coordinate system must be used to resolve the load on the "lug" bolts. The Z' and Y' components are:

$$R_z' = R_z \cos\theta + R_y \sin\theta$$

$$R_y' = R_y \cos\theta + R_z \sin\theta$$

The load on the corner bolt is by superposition the sum of the loads due to the forces R_Z', R_Y', and R_X. The bolt loads due to all of the lug reactions are:

$$FT = (R_z \cos\theta + R_y \sin\theta)\left(1/5 + \frac{\bar{x}\,x}{I'_y} + \frac{\bar{y}\,y}{I'_x}\right) + (R_y \cos\theta - R_z \sin\theta)\left(\frac{\bar{Z}_1\,y}{I'_x}\right) + \frac{R_x\,Z_2\,x}{I'_y}$$

$$FT = R_z\left(\frac{\cos\theta}{5} + \frac{\bar{x}\,x\cos\theta}{I'_y} + \frac{\bar{y}\,y\cos\theta - \bar{Z}_1 y\sin\theta}{I'_x}\right) + R_y\left(\frac{\sin\theta}{5} + \frac{\bar{x}\,x\sin\theta}{I'_y} + \frac{\bar{y}\,y\sin\theta + \bar{Z}_1 y\cos\theta}{I'_x}\right) + R_x\left(\frac{Z_2\,X}{I'_y}\right) \qquad \text{eq 3.5-1}$$

where $\bar{x}$ = distance from the Z' component of the lug reaction to the centroid of the bolt pattern.

x = distance from the aft edge to the forward corner bolt (or vice versa because of pattern symmetry).

$\bar{y}$ = distance from the Z' component of the lug reaction to the centroid of the bolt pattern.

y = distance from the left edge to the right corner bolt (or vice versa because of pattern symmetry).

$I'_y = \sum dx_i^2$

dx_i = distance of the ith bolt from the aft (or forward) edge of the lug.

$I'_x = d_{yi}^2$

d_{yi} = distance of the ith bolt from the left (or right) edge of the lug.

$Z' = H+H1$

$Z_2 = C+H1$

R_x, R_y, R_z = lug reactions limit load per table XI

These equations are derived for any of the lugs or the button or the hook. A sketch of each lug is shown in figure 8

Equation 3.5-1 can be rewritten as

$$FT_i = R_x/B_x + R_y/B_y + R_z/B_z$$

The values of B_x, B_y and B_z can be calculated from equation 3.5-1 and the geometric data in Table XV. The values for B_x, B_y, and B_z for each lug are listed at the bottom of that table. Table XVI gives the values of B_x, B_y and B_z which are appropriate for each mounting configuration.

Once the maximum screw tension FT_j is known for the jth lug, the margin of safety is calculated as follows:

$$MSY_j = \frac{FFY}{SFY\,(FT_j)} - 1$$

$$MSU_j = \frac{FFU}{1.5\,(FT_j)} - 1$$

$$MSYT_j = \frac{FFY\,(CTY)}{SFY\,(FT_j)} - 1$$

$$MSUT_j = \frac{FFU\,(CTU)}{1.5\,(FT_j)} - 1$$

TABLE XVI

QRC335 +GEN. LUG SCREW DATA

	FORWARD LUG				AFT LUG	
CONF.	BZ	BX	BY	BZ	BX	BY
A	5.00	6.11	8.78	5.00	6.11	8.78
B	5.00	3.46	4.55	5.00	3.46	4.55
C	5.00	6.11	8.78	5.00	6.11	8.78
D	5.00	3.46	4.55	5.00	3.46	4.55
G	-1.00	-1.00	-1.00	-1.00	-1.00	-1.00

QRC335 'WELL LUG SCREW DATA

	FORWARD LUG				AFT LUG	
CONF.	BZ	BX	BY	BZ	BX	BY
E	4.54	3.57	4.81	1.13	11.22	1.54
F	-1.00	-1.00	-1.00	-1.00	-1.00	-1.00

Lug Screw Coefficients

where

FFY = FFU = screw and insert tensils load capability = 8300 lb

SFY = yield safety factor = 1.15

CTY = CTU = temperature degradation factor = .97

3.5.1 Example of Lug Screw Margins

As an example, the lug screw margins will be calculated for load case E17 point 43, forward lug screws (Button screws). From table XI,

$$R_x = 0$$

$$R_y = -5616$$

$$R_z = 13100$$

From tables XVI

$$B_x = 3.57$$

$$B_y = 4.81$$

$$B_z = 4.53$$

Therefore

$$FT_{43} = \frac{0}{3.57} + \frac{-5616}{4.81} + \frac{13100}{4.53}$$

$$= 0 + 1166 + 2887 = 4053$$

Then

$$MSY = \frac{8300}{1.15\ (4053)} -1 = 1.78-1 = .78$$

$$MSU = \frac{8300}{1.5\ (4053)} -1 = 1.37-1 = .37$$

$$MSYT = \frac{8300\ (.97)}{1.5\ (4053)} = .32$$

These margins agree with the computer answers in table XIV.

SECTION IV

INTERNAL BENDING MOMENT AND MARGINS AT JOINTS

4.1 METHOD OF ANALYSIS

Failure of a joint by rivet (or screw) shear, rivet bearing, skin tearing or failure of the ring or V-band clamp by the stresses at the root of the groove are all calculated based on the internal bending moment at the joint. Internal shear forces produce negligible stress at the joints. Therefore, the bending moment at each joint for each load case is computed and tabulated. From geometric data on each joint, such as rivet diameter and spacing, the bending moment required to yield and the bending moment required to rupture each joint by each of the various possible methods is calculated using the equations derived in appendix V. The actual bending moments at the joints and their bending moment capabilities are computed for both the vertical plane and the horizontal plane. Margins of safety are then computed by comparing the vector sum of the horizontal bending moment and vertical bending moment to the lesser of the horizontal or vertical moment capability.

4.2 EXTERNAL LOAD DISTRIBUTIONS AND INTERNAL SHEAR-MOMENT DISTRIBUTIONS.

Aside from the local distortions, the pod acts as a beam, the length of the beam being the length of the pod and the stiffness being determined by the I of the cross section. Hence, it is advisable to construct shear and moment diagrams to determine where the maximum loads occur. This requires additional inputs concerning the distribution of mass and aerodynamic forces.

For computation purposes, it has been assumed that the mass distribution forward of the CG is constant and that the mass distribution aft of the CG is also constant but of a different amplitude. The amplitudes of the two sections were selected such that their CG and moment of inertia equal that estimated for the pod as given in appendix I.

Aerodynamic forces are assumed to be sine wave distributions with a wave-length equal to twice the pod length. Aerodynamic moments are assumed to be sine wave distributions with a wave-length equal to the pod length.

Using these distributions, each of the basic loads from tables V and VI was calculated as a distributed load, and all were summed to give a horizontal load distribution and a vertical load distribution. Each of these distributions was integrated, with appropriate jumps at each sway brace or lug for the component of the concentrated force, to give the horizontal and vertical shear distributions.

The shear diagrams were integrated to produce the horizontal and vertical bending moment distributions. A typical shear and bending moment distribution is given in table XVII for case A2.

4.2.1 Shear Loads

Shear loads at critical locations are listed in tables XVIII, XIX, and XX for each load case. The largest shear occurs in load case G7, the jettison load, at the jettison foot. The largest shear for a flight load occurs for load case E17, an F-4 forward fuselage installation load. These values are for limit loads. For ultimate loads all values are 50 percent greater except for jettison cases F8 and G7 where a smaller factor of safety (1.15) is appropriate.

4.2.2 Bending Moments

Bending moments at critical locations are listed in tables XXI, XXII and XXIII for each load case. The largest moment occurs in load case G7, the jettison load. The largest moment for a flight load occurs for load case E17. This case is for a pod mounted at the forward missile station of the F-4C. These values are for limit loads. For ultimate loads all values are 50 percent greater, except for jettison as explained above.

TABLE XVII
SHEAR AND MOMENT DISTRIBUTION FOR CASE A2

CASE A 2 FOR WRC335 +GEN.

X	VH	VV	VT	MH	MV	MT
.00000	.00000	.00000	.00000	.00000	.00000	.00000
2.00000	3.50417	3.61292	5.03313	2.33664	2.40974	4.35660
4.00000	13.99706	14.40215	20.08332	18.67689	19.23808	26.81287
6.00000	31.42013	32.21960	45.00363	62.94616	64.70589	90.27221
8.00000	55.67629	56.82053	79.55137	148.91361	152.64091	213.24753
10.00000	115.09446	88.53562	145.20775	304.34942	286.17585	417.76211
12.00000	209.50345	81.34857	224.74270	627.87560	416.94450	753.70447
14.00000	310.23319	79.60482	320.28355	1146.57790	545.91981	1269.90910
16.00000	417.04410	82.71475	425.16762	1872.86320	683.06346	1993.53770
18.00000	529.66528	90.01835	537.26025	2818.62880	837.08666	2940.30300
20.00000	647.79674	100.79341	655.59126	3995.19880	1015.31640	4122.19330
22.00000	771.11201	114.26457	779.53199	5413.27280	1223.58030	5549.83510
24.00000	899.26082	129.61293	908.55354	7082.87000	1466.11150	7233.01630
26.00000	1031.87180	145.98641	1042.14750	9013.29080	1745.46880	9180.74360
28.00000	1168.55580	162.51019	1179.80170	11213.07300	2062.48240	11401.17600
30.00000	1308.90870	178.29789	1320.99660	13689.95930	2416.22110	13901.54940
32.00000	1452.51470	192.46263	1465.21000	16450.87500	2803.97640	16688.12600
34.00000	1598.94960	204.12812	1611.92680	19501.90500	3221.27600	19766.15400
36.00000	1747.78420	212.43978	1760.64760	22848.27500	3661.91530	23139.86100
38.00000	1898.58700	216.57562	1910.89970	26494.35400	4118.01010	26812.47300
40.00000	2050.92790	215.75654	2062.24540	30443.64800	4580.07470	30786.24400
42.00000	2204.38110	209.25646	2214.29090	34698.80700	5037.11500	35062.50900
44.00000	2358.52780	196.41147	2366.69200	39261.63400	5476.74750	39641.77800
46.00000	2512.95950	176.62859	2519.15920	44133.10800	5885.32880	44523.79200
48.00000	2667.28000	149.39342	2671.46040	49313.39800	6248.10720	49707.64700
50.00000	-1964.33250	-6720.04130	7001.25370	53653.39400	4909.15050	53877.51000
52.00000	-1811.35980	-6763.37660	7001.73450	49877.87400	-8536.16720	50603.04800
54.00000	-1963.00910	-1757.22490	2634.62400	6036.57300	-23080.18500	51498.16500
56.00000	-1827.96780	-1805.59430	2569.36500	42245.87500	-26641.54500	49944.82600
58.00000	-1694.75160	-1862.71760	2518.31290	38723.48400	-30308.40000	49174.25500
60.00000	-1563.63830	-1928.53230	2482.78090	35465.46500	-34098.21300	49198.44800
62.00000	-1434.88110	-2002.87250	2463.81450	32467.36000	-38028.21600	50002.74300
64.00000	-1308.70860	-2085.47100	2462.09410	29724.21900	-42115.21100	51548.22800
66.00000	-1185.32400	-2175.96170	2477.86230	27230.66700	-46375.36600	53779.02500
68.00000	-939.58469	3212.82250	3347.39420	25136.34100	-44020.49800	50691.61400
70.00000	-1495.09440	2147.15180	2616.40360	23213.52900	-37929.16500	44468.97100
72.00000	-1381.04300	2036.11010	2460.28940	20337.94300	-33744.91900	39399.88900

TABLE XVII (Continued)

74.00000	-1270.34480	1919.53970	2301.82710	17687.12000	-29788.41100	34643.66800
76.00000	-1163.08250	1798.22360	2141.58100	15254.27180	-26069.92700	30204.86300
78.00000	-1059.31770	1673.00510	1980.17680	13032.46100	-22598.11800	26086.77700
80.00000	-959.09213	1544.77850	1818.29550	11014.64270	-19379.91300	22291.33000
82.00000	-862.42934	1414.47880	1656.66370	9193.71420	-16420.38600	18818.96300
84.00000	-769.33645	1283.07070	1496.04450	7562.54610	-13722.73530	15668.61580
86.00000	-679.80623	1151.53810	1337.22720	6113.99350	-11288.18270	12837.60010
88.00000	-593.81863	1020.87200	1181.01650	4840.95640	-9116.00240	10321.64500
90.00000	-511.34352	892.05986	1028.22310	3736.37790	-7203.45970	8114.82300
92.00000	-432.34206	766.07329	879.65214	2793.27120	-5545.87790	6209.59940
94.00000	-356.76900	643.85746	736.09547	2004.72620	-4136.65180	4596.82640
96.00000	-284.57516	526.31962	598.32714	1363.93940	-2967.33180	3265.79030
98.00000	-215.70858	414.31889	467.10847	864.20575	-2027.68360	2204.16690
100.00000	-150.11708	308.65605	343.22541	498.92218	-1305.82640	1397.89340
102.00000	-87.74976	210.06425	227.65546	261.58777	-788.34228	830.60923
104.00000	-41.07467	130.53996	136.84958	142.05090	-457.01855	478.58585
106.00000	-26.73629	85.88872	89.95388	74.75488	-242.04199	253.32315
108.00000	-15.49276	50.19352	52.53013	33.04565	-107.49170	112.45657
110.00000	-7.31307	23.84037	24.93680	10.74689	-35.04053	36.65152
112.00000	-2.17391	7.11478	7.43949	1.76459	-5.70898	5.97547
114.00000	-.06026	.19779	.20677	.03302	-.04102	.05266

TABLE XVIII

QRC335 +GEN.HORIZONTAL SHEAR (LIMIT LOADS)

Load Case	STA. FOR MAX	MAX VALUE	JOINTI X= 17.5	JOINT2 X= 31.8	JOINT3 X= 41.8	JOINT4 X= 96.8
A 1	49	1833	307	919	1442	-145
A 2	49	2744	501	1438	2189	-256
A 3	49	-857	-145	-430	-672	96
A 4	53	-4357	440	1245	1825	274
A 5	70	-1322	242	663	985	-270
A 6	67	-252	7	13	8	34
B 1	58	-2383	307	919	1442	-145
B 2	58	-3508	501	1438	2189	-256
B 3	58	1097	-145	-430	-672	96
B 4	78	-3135	440	1246	1825	274
B 5	58	-1473	242	663	985	-270
B 6	78	-100	7	13	8	34
C 9	53	312	-40	-117	-179	-7
C10	50	-1168	180	533	835	-112
C11	53	742	-86	-249	-374	-31
C12	53	175	-27	-84	-131	4
C13	50	-858	91	292	484	-73
C14	50	-787	84	269	445	-67
D 9	52	254	-40	-117	-179	-7
D10	46	968	180	533	835	-112
D11	52	549	-86	-249	-374	-31
D12	52	174	-27	-84	-131	4
D13	51	660	91	292	484	-73
D14	51	606	84	269	445	-67
G 7	51	0	0	0	0	0

QRC335 'WELLHORIZONTAL SHEAR (LIMIT LOADS)

Load Case	STA. FOR MAX	MAX VALUE	JOINT1 X= 17.5	JOINT2 X= 27.5	JOINT3 X= 82.5
E15	81	-1490	179	363	147
E16	81	491	-81	-167	-70
E17	81	-3687	127	230	272
E18	81	2364	-76	-137	-204
F 8	81	0	0	0	0

TABLE XIX

QRC335 +GEN.VERTICAL SHEAR (LIMIT LOADS)

Load Case	STA. FOR MAX	MAX VALUE	JOINT1 X= 17.5	JOINT2 X= 31.8	JOINT3 X= 41.8	JOINT4 X= 96.8
A 1	52	-5464	-89	-284	-473	582
A 2	52	-6762	88	191	210	481
A 3	70	3583	-80	-184	-222	-437
A 4	52	-6263	-260	-708	-1024	91
A 5	52	-4014	-174	-456	-647	196
A 6	70	2632	-166	-478	-699	-219
B 1	53	7001	-89	-284	-473	582
B 2	53	9087	88	191	210	481
B 3	58	3832	-80	-184	-222	-437
B 4	53	7789	-260	-708	-1024	91
B 5	53	4861	-174	-456	-647	196
B 6	78	1687	-166	-478	-699	-219
C 9	53	1625	-93	-292	-458	-110
C10	52	-4471	-222	-617	-917	185
C11	70	2067	-113	-339	-513	-161
C12	53	1655	-91	-283	-438	-128
C13	52	-3686	-306	-838	-1208	-25
C14	52	-3481	-300	-822	-1184	-20
D 9	47	1532	-93	-292	-458	-110
D10	47	3837	-222	-617	-917	185
D11	47	2293	-113	-339	-513	-161
D12	47	1430	-91	-283	-438	-128
D13	47	3438	-306	-838	-1208	-25
D14	47	3237	-300	-822	-1184	-20
G 7	51	8316	1683	4514	6494	-957

QRC335 'WELLVERTICAL SHEAR (LIMIT LOADS)

Load Case	STA. FOR MAX	MAX VALUE	JOINT1 X= 17.5	JOINT2 X= 27.5	JOINT3 X= 82.5
E15	56	1852	-133	-290	142
E16	31	124	52	107	-6
E17	56	6631	-182	-422	291
E18	81	3375	-19	-27	-113
F 8	80	2320	-562	-92	-895

TABLE XII

QRC335 *GEN. TOTAL SHEAR (LIMIT LOADS)

Load Case	STA. FOR MAX	MAX VALUE	JOINT1 X= 17.5	JOINT2 X= 31.8	JOINT3 X= 41.8	JOINT4 X= 96.8
A 1	52	5607	320	962	1518	600
A 2	50	7002	509	1451	2199	545
A 3	70	3591	167	469	709	448
A 4	52	6375	512	1433	2093	289
A 5	52	4102	299	805	1179	334
A 6	70	2633	167	479	700	222
B 1	53	7081	320	962	1518	600
B 2	53	9228	509	1451	2199	545
B 3	58	3888	167	469	709	448
B 4	53	7803	512	1433	2093	289
B 5	53	4954	299	805	1179	334
B 6	78	1690	167	479	700	222
C 9	53	1655	103	316	493	111
C10	52	4605	287	816	1241	217
C11	53	2192	143	422	636	166
C12	53	1664	97	297	458	129
C13	52	3775	320	989	1303	79
C14	52	3560	313	866	1266	71
D 9	47	1536	103	316	493	111
D10	47	3919	287	816	1241	217
D11	47	2299	143	422	636	166
D12	47	1433	97	297	458	129
D13	47	3485	320	989	1303	79
D14	47	3278	313	866	1266	71
G 7	51	8316	1683	4514	6494	958

QRC335 *WELL TOTAL SHEAR (LIMIT LOADS)

Load Case	STA. FOR MAX	MAX VALUE	JOINT1 X= 17.5	JOINT2 X= 27.5	JOINT3 X= 82.5
E15	56	2148	224	465	204
E16	61	492	97	199	72
E17	56	7203	223	481	399
E18	81	4121	79	141	234
F 8	80	2320	563	93	896

TABLE XXI

QRC335 +GEN.HORIZONTAL MOMENT (LIMIT LOADS)

Load Case	STA. FOR MAX	MAX VALUE	JOINT1 X= 17.5	JOINT2 X= 31.8	JOINT3 X= 41.8	JOINT4 X= 96.8
A 1	50	35211	1738	10243	22011	784
A 2	50	54127	2561	16162	34259	1147
A 3	50	-16460	-778	-4790	-10289	-490
A 4	50	45932	2639	14455	29870	-1673
A 5	50	24592	964	7416	15629	1200
A 6	70	-2826	42	189	300	-205
B 1	58	47002	1738	10243	22011	784
B 2	58	71751	2561	16162	34259	1147
B 3	58	-22200	-778	-4790	-10289	-490
B 4	58	55314	2639	14455	29870	-1673
B 5	58	33778	964	7416	15629	1200
B 6	78	-1125	42	189	300	-205
C 9	50	-4456	-241	-1349	-2842	49
C10	50	20400	974	5932	12748	585
C11	50	-9339	-518	-2872	-6003	197
C12	50	-3225	-168	-951	-2031	-18
C13	50	11566	570	3188	7047	466
C14	50	10636	525	2932	6481	427
D 9	52	-4377	-241	-1349	-2842	49
D10	52	21668	974	5932	12748	585
D11	52	-8961	-518	-2872	-6003	197
D12	52	-3298	-168	-951	-2031	-18
D13	52	12818	570	3188	7047	466
D14	52	11783	525	2932	6481	427
G 7	52	0	0	0	0	0

QRC335 'WELLHORIZONTAL MOMENT (LIMIT LOADS)

Load Case	STA. FOR MAX	MAX VALUE	JOINT1 X= 17.5	JOINT2 X= 27.5	JOINT3 X= 82.5
E15	56	30819	864	3604	-1130
E16	56	-9189	-418	-1676	518
E17	56	79154	570	2416	-1870
E18	56	-49390	-398	-1507	1318
F 8	56	0	0	0	0

TABLE XXIII

QRC335 +GEN.TOTAL MOMENT (LIMIT LOADS)

Load Case	STA. FOR MAX	MAX VALUE	JOINT1 X= 17.5	JOINT2 X= 31.8	JOINT3 X= 41.8	JOINT4 X= 96.8
A 1	67	59412	1739	10583	22877	3002
A 2	67	54793	2682	16396	34621	2810
A 3	70	35882	1102	5463	11387	2335
A 4	53	63740	2899	16573	34261	1689
A 5	53	36412	1134	9037	18929	1432
A 6	53	26933	1141	5634	11572	1226
B 1	58	48683	1739	10583	22877	3002
B 2	58	83797	2682	16396	34621	2810
B 3	53	24852	1102	5463	11387	2335
B 4	53	62411	2899	16573	34261	1689
B 5	53	34717	1134	9037	18929	1432
B 6	53	28089	1141	5634	11572	1226
C 9	53	18965	768	3628	7682	534
C10	53	40804	1377	9132	19384	986
C11	53	23909	995	4902	10220	862
C12	53	18135	739	3426	7215	637
C13	53	46542	1662	10201	21169	620
C14	53	44963	1613	9946	20619	575
D 9	47	14603	768	3628	7682	534
D10	47	26826	1377	9132	19384	986
D11	47	17884	995	4902	10220	862
D12	47	14339	739	3426	7215	637
D13	47	32662	1662	10201	21169	620
D14	47	31652	1613	9946	20619	575
G 7	51	176632	7153	51462	106505	3160

QRC335 +WELLTOTAL MOMENT (LIMIT LOADS)

Load Case	STA. FOR MAX	MAX VALUE	JOINT1 X= 17.5	JOINT2 X= 27.5	JOINT3 X= 82.5
E15	56	51369	995	4460	1245
E16	56	9200	467	1956	524
E17	56	173519	976	4492	2357
E18	56	93069	415	1553	1495
F 8	57	18448	645	1721	2958

4.3 DATA FOR JOINTS

The geometric and material data needed for calculating the bending moment that would yield or rupture the joints per the methods of appendix V is given in tables XXIV, XXV, XXVI and XXVII.

4.4 MOMENT CAPABILITIES OF JOINTS

The internal bending moment that would yield or rupture (ultimate failure) each joint by each possible failure method is given in tables XXVIII and XXIX. Values are included for both the horizontal and vertical direction. All bending moments are in kilo-inch-pounds.

4.5 MARGINS OF SAFETY OF JOINTS

The margins of safety at each joint for each load case were calculated by the following equations:

$$MSY_j = \frac{FFY_j}{SFY\ (FT_j)} - 1$$

$$MSU_j = \frac{FFU_j}{1.5\ (FT_j)} - 1$$

$$MSYT_j = \frac{FFY_j\ (CTY)}{SFY\ (FT_j)} - 1$$

$$MSUT_j = \frac{FFU_j\ (CTU)}{1.5\ (FT_j)} - 1$$

where

FFY_j = lesser of "HOR.YIELD" or "VERT. YIELD" from moment capability table for jth joint and failure method.

FFU_j = lesser of "HOR. ULT." or "VERT. ULT." from moment capability table for jth joint and failure method.

SFY = yield safety factor = 1.15

TABLE XXIV

DIMENSIONAL DATA FOR RIVETS AND RINGS

QRC335 *GEN. RIVET DATA -GENERAL

NO.	STA.	LOC.	SKIN MATL.	SKIN THICK	RIVET DIA.	RIVET ROWS	HEAD DEPTH	RIVET STRENGTH	BEARING DERATING
23	16.1	NOSE	3-ALUM.	.100	.180	1	.010	936.	1.000
25	18.9	GEN.A	4-ALUM.	.058	.190	1	.060	2126.	1.000
26	30.4	GEN.B	4-ALUM.	.183	.250	1	.090	3682.	.900
28	33.2	SERV.A	3-ALUM.	.125	.125	1	.040	530.	1.000
29	40.4	SERV.B	3-ALUM.	.125	.125	1	.040	530.	1.000
31	43.2	PRIN.A	3-ALUM.	.100	.125	1	.040	530.	1.000
32	94.9	PRIN.B	3-ALUM.	.100	.125	3	.040	530.	1.000
40	98.2	TAIL	3-ALUM.	.100	.180	1	.010	936.	1.000

LONG./HARD. SCREW DIA.= .190

QRC335 *WELL RIVET DATA -GENERAL

NO.	STA.	LOC.	SKIN MATL.	SKIN THICK	RIVET DIA.	RIVET ROWS	HEAD DEPTH	RIVET STRENGTH	BEARING DERATING
23	16.1	NOSE	3-ALUM.	.100	.180	1	.010	936.	1.000
28	18.9	SERV.A	3-ALUM.	.125	.125	1	.040	530.	1.000
29	26.1	SERV.B	3-ALUM.	.125	.125	1	.040	530.	1.000
31	28.9	PRIN.A	3-ALUM.	.100	.125	1	.040	530.	1.000
32	80.6	PRIN.B	3-ALUM.	.100	.125	3	.040	530.	1.000
40	83.9	TAIL	3-ALUM.	.100	.180	1	.010	936.	1.000

LONG./HARD. SCREW DIA.= .190

TABLE XXV

QRC335 +GEN. RIVET DATA - HORIZONTAL

NO.	STA.	LOC.	N.A. POS.	QS	RIVET SPACING	NO. SCREW	SCREW DIST.	SCREW STRENGTH
23	16.1	NOSE	2.500	1.000	1.560	0	.00	0.
25	18.9	GEN.A	2.500	1.000	3.440	0	.00	0.
26	30.4	GEN.B	2.500	1.000	5.130	0	.00	0.
28	33.2	SERV.A	2.500	1.000	1.600	0	.00	0.
29	40.4	SERV.B	2.500	.500	.780	0	.00	0.
31	43.2	PRIN.A	2.500	.515	.420	11	2.86	2695.
32	94.9	PRIN.B	1.000	.635	.560	27	1.55	2695.
40	98.2	TAIL	2.500	1.000	1.560	0	.00	0.

QRC335 +WELL RIVET DATA - HORIZONTAL

NO.	STA.	LOC.	N.A. POS.	QS	RIVET SPACING	NO. SCREW	SCREW DIST.	SCREW STRENGTH
23	16.1	NOSE	2.500	1.000	1.560	0	.00	0.
28	18.9	SERV.A	2.500	1.000	1.600	0	.00	0.
29	26.1	SERV.B	2.500	.500	.780	0	.00	0.
31	28.9	PRIN.A	2.500	.515	.420	11	2.86	2695.
32	80.6	PRIN.B	1.000	.635	.560	27	1.55	2695.
40	83.9	TAIL	2.500	1.000	1.560	0	.00	0.

TABLE XXVI

QRC335 +GEN. RIVET DATA - VERTICAL

NO.	STA.	LOC.	N.A. POS.	QS	RIVET SPACING	NO. SCREW	SCREW DIST.	SCREW STRENGTH
23	16.1	NOSE	2.500	1.000	1.560	0	.00	0.
25	18.9	GEN.A	2.500	1.000	3.440	0	.00	0.
26	30.4	GEN.B	2.500	1.000	5.130	0	.00	0.
28	33.2	SERV.A	2.500	1.000	1.600	0	.00	0.
29	40.4	SERV.B	2.500	.500	.780	0	.00	0.
31	43.2	PRIN.A	4.000	.530	.420	11	2.14	2695.
32	94.9	PRIN.B	4.000	.530	.560	27	3.59	2695.
40	98.2	TAIL	2.500	1.000	1.560	0	.00	0.

QRC335 +WELL RIVET DATA - VERTICAL

NO.	STA.	LOC.	N.A. POS.	QS	RIVET SPACING	NO. SCREW	SCREW DIST.	SCREW STRENGTH
23	16.1	NOSE	2.500	1.000	1.560	0	.00	0.
28	18.9	SERV.A	2.500	1.000	1.600	0	.00	0.
29	26.1	SERV.B	2.500	.500	.780	0	.00	0.
31	28.9	PRIN.A	4.000	.530	.420	11	2.14	2695.
32	80.6	PRIN.B	4.000	.530	.560	27	3.59	2695.
40	83.9	TAIL	2.500	1.000	1.560	0	.00	0.

TABLE XXVII

QRC335 +GEN. RING DATA

NO.	STA.	LOC.	MATERIAL	RR	TO	U	MU
24	17.5	NOSE	7-ALUM.	4.660	.115	.227	.330
24	17.5	GEN.A	4-ALUM.	4.660	.215	.277	.330
27	31.8	GEN.B	4-ALUM.	4.660	.215	.277	.330
27	31.8	SERV.A	6-ALUM.	4.660	.360	.350	.330
30	41.8	SERV.B	1-STEEL	4.722	.220	.342	.360
30	41.8	PRIN.A	1-STEEL	4.722	.120	.292	.360
39	96.8	PRIN.B	1-STEEL	4.722	.250	.357	.360
39	96.8	TAIL	6-ALUM.	4.660	.115	.227	.330
99	41.8	V-BAND	1-STEEL	4.722	.170	.198	.360

QRC335 'WELL RING DATA

NO.	STA.	LOC.	MATERIAL	RR	TO	U	MU
24	17.5	NOSE	7-ALUM.	4.660	.115	.227	.330
27	17.5	SERV.A	6-ALUM.	4.660	.360	.353	.330
30	27.5	SERV.B	1-STEEL	4.722	.220	.342	.360
30	27.5	PRIN.A	1-STEEL	4.722	.120	.292	.360
39	82.5	PRIN.B	1-STEEL	4.722	.250	.357	.360
39	82.5	TAIL	7-ALUM.	4.660	.115	.227	.330
99	27.5	V-BAND	1-STEEL	4.722	.170	.198	.360

QRC335 +GEN. MOMENT CAPABILITY - RIVET SHEAR

NO.	STA.	LOC.	HOR.YIELD	HOR.ULT.	VERT.YIELD	VERT.ULT.
23	16.1	NOSE	62.8	62.8	62.8	62.8
25	18.9	GEN.A	64.7	64.7	64.7	64.7
26	30.4	GEN.B	75.2	75.2	75.2	75.2
28	33.2	SERV.A	1000.0	1000.0	1000.0	1000.0
29	40.4	SERV.B	142.3	142.3	142.3	142.3
31	43.2	PRIN.A	174.9	174.9	135.0	135.0
32	94.9	PRIN.B	308.7	308.7	555.7	555.7
40	98.2	TAIL	62.8	62.8	62.8	62.8

QRC335 +GEN. MOMENT CAPABILITY - RIVET BEARING

NO.	STA.	LOC.	HOR.YIELD	HOR.ULT.	VERT.YIELD	VERT.ULT.
23	16.1	NOSE	84.9	142.3	84.9	142.3
25	18.9	GEN.A	11.0	18.8	11.0	18.8
26	30.4	GEN.B	43.1	73.5	43.1	73.5
28	33.2	SERV.A	1000.0	1000.0	1000.0	1000.0
29	40.4	SERV.B	260.8	437.0	260.8	437.0
31	43.2	PRIN.A	173.4	290.6	133.8	224.2
32	94.9	PRIN.B	572.4	959.1	848.7	1422.1
40	98.2	TAIL	84.9	142.3	84.9	142.3

QRC335 +GEN. MOMENT CAPABILITY - SKIN TEARING

NO.	STA.	LOC.	HOR.YIELD	HOR.ULT.	VERT.YIELD	VERT.ULT.
23	16.1	NOSE	395.7	593.6	395.7	593.6
25	18.9	GEN.A	222.6	333.9	222.6	333.9
26	30.4	GEN.B	720.0	1080.0	720.0	1080.0
28	33.2	SERV.A	280.0	380.0	404.0	404.0
29	40.4	SERV.B	916.5	1374.7	916.5	1374.7
31	43.2	PRIN.A	561.7	842.6	591.8	887.7
32	94.9	PRIN.B	454.6	681.8	674.0	1011.0
40	98.2	TAIL	395.7	593.6	395.7	593.6

QRC335 +GEN. MOMENT CAPABILITY OF RINGS

NO.	STA.	LOC.	YIELD MOM	ULT. MOM
24	17.5	NOSE	47.9	57.4
24	17.5	GEN.A	150.5	225.7
27	31.8	GEN.B	150.5	225.7
27	31.8	SERV.A	225.3	306.8
30	41.8	SERV.B	507.1	542.1
30	41.8	PRIN.A	183.1	195.7
39	96.8	PRIN.B	622.0	664.9
39	96.8	TAIL	38.3	52.0
99	41.8	V-BAND	506.6	541.6

TABLE XXIX

QRC335 'WELL MOMENT CAPABILITY - RIVET SHEAR

NO.	STA.	LOC.	HOR.YIELD	HOR.ULT.	VERT.YIELD	VERT.ULT.
23	16.1	NOSE	62.8	62.8	62.8	62.8
28	18.9	SERV.A	1000.0	1000.0	1000.0	1000.0
29	26.1	SERV.B	142.3	142.3	142.3	142.3
31	28.9	PRIN.A	174.9	174.9	135.0	135.0
32	80.6	PRIN.B	308.7	308.7	555.7	555.7
40	83.9	TAIL	62.8	62.8	62.8	62.8

QRC335 'WELL MOMENT CAPABILITY - RIVET BEARING

NO.	STA.	LOC.	HOR.YIELD	HOR.ULT.	VERT.YIELD	VERT.ULT.
23	16.1	NOSE	84.9	142.3	84.9	142.3
28	18.9	SERV.A	1000.0	1000.0	1000.0	1000.0
29	26.1	SERV.B	260.8	437.0	260.8	437.0
31	28.9	PRIN.A	173.4	290.6	133.8	224.2
32	80.6	PRIN.B	572.4	959.1	848.7	1422.1
40	83.9	TAIL	84.9	142.3	84.9	142.3

QRC335 'WELL MOMENT CAPABILITY - SKIN TEARING

NO.	STA.	LOC.	HOR.YIELD	HOR.ULT.	VERT.YIELD	VERT.ULT.
23	16.1	NOSE	395.7	593.6	395.7	593.6
28	18.9	SERV.A	280.0	380.0	404.0	404.0
29	26.1	SERV.B	916.5	1374.7	916.5	1374.7
31	28.9	PRIN.A	561.7	842.6	591.8	887.7
32	80.6	PRIN.B	454.6	681.8	674.0	1011.0
40	83.9	TAIL	395.7	593.6	395.7	593.6

QRC335 'WELL MOMENT CAPABILITY OF RINGS

NO.	STA.	LOC.	YIELD MOM	ULT. MOM
24	17.5	NOSE	47.9	57.4
27	17.5	SERV.A	223.7	303.5
30	27.5	SERV.B	507.1	542.1
30	27.5	PRIN.A	183.1	195.7
39	82.5	PRIN.B	622.0	664.9
39	82.5	TAIL	47.9	57.4
99	27.5	V-BAND	506.6	541.6

FT_j = vector sum of actual horizontal bending moment and vertical bending moment for limit load at jth joint. (Total Moment per table XXIII).

CTY = temperature derating factor for yield stress per table XXXIII, appendix IV depending upon appropriate material.

CTU = temperature derating factor for ultimate stress per table XXXIII, appendix IV depending upon appropriate material.

Margins of safety for joints appear in table XIV for a typical load case and in summary tables I and II for locations whose numbers are 23 to 40 inclusively.

SECTION V
SKIN STRESSES

5.1 METHODS OF ANALYSIS

The concentrated forces at the sway braces cause high local stress areas. At these areas the stress caused by tangential bending (distortion of cross-sectional shape) is much higher than the stress caused by simple beam bending stresses (axial). This local stress is very complex because of the changing thickness of the re-inforcing hardback. All attempts to calculate the local stress have resulted in very poor correlation with test results. Consequently, the test described in reference 1 was conducted to establish a semi-empirical method for calculating the local skin stresses.

The referenced test used a 669A pod structure that was covered with a photoelastic coating that enabled measurement of the maximum shear stress and its orientation at any point on the surface of the pod skin. The test started with a survey that located the ten most critical spots on the pod skin. Some of these locations were most critical for pitching moments, some for side force etc. Consequently, it is not possible to define the most critical location until an actual load condition is defined.

The test then proceeded to meaure the stress at each critical location for unit load components of:

1) positive yawing moment
2) negative yawing moment
3) positive side force
4) negative side force
5) positive vertical force
6) negative vertical force
7) positive pitching moment
8) negative pitching moment

In general the internal stress distribution is entirely different for positive and negative loads components so the distinction shown above is necessary.

By means of equations derived in reference 1, the data was reduced to the shear stress and tangential bending stress at each location for each load component. This data reduction includes the effects of simple beam bending stress. The data reduction also calculates the tangential stress at the inside of the skin, because this is sometimes more critical than the stress at the outside of the skin. Because these stresses are computed for a unit load component, they are called stress coefficients. The stress due to an actual load component is the product of the corresponding coefficient and the magnitude of the load component. For combined loads, it is assumed that shear stresses add algebraically and that tangential stresses add algebraically.

These stress coefficients and the detail procedure for using them to calculate skin stresses is given in appendix VI.

5.2 MARGINS OF SAFETY FOR SKIN LOCATIONS

The net resultant limit loads, table lX, were used with the equations in appendix Vl to calculate the margins of safety for each of the ten critical skin locations and for each load case. Both the margin of safety at the outside of the skin and at the inside of the skin were calculated. These critical skin locations are points 11 to 20 inclusive in table XlV. None of the skin locations had any margins less than 0.6, so no skin locations appear in the summary tables I and II.

SECTION VI

SPECIAL CONSIDERATIONS

The only significant difference in construction of the QRC-335A structure and the earlier 669A structure, is in the construction of the adapter modules. A careful check was made to determine that the joint strengths for the adapter are really the most critical stress in the adapter for static loads. This was found to be true, so this report, which includes critical lug stresses, critical joint stresses, and critical skin stresses, includes all critical stress locations.

SECTION VII
CONCLUSIONS

Three mounting configurations have been studied: one with a RATG and with 30-inch lug spacing; another with a RATG and with 14-inch lug spacing; and a third without a RATG and with lugs to mate with the Sparrow launcher. Each configuration was studied for yielding and rupture corresponding to room temperature strength and elevated temperature strength. Twelve flight loads were considered for each of the first two configurations and four flight loads for the last. Furthermore jettison loads were considered for all configurations. Because of the quantity of computations, the matrix multiplication and margin of safety computations were done by computer.

The critical margins of safety for the configurations with a RATG for all loads are given in Table I. For the configuration without the RATG critical margins are given in Table II.

The critical margins of safety listed in tables I and II were arbitrarily selected to be those less than 0.6. Since there were no margins less than 0.6 for the flight loads for the configuration with generator, only the jettison case G7 appears in the Table. Of the negative margins of safety, all but one are irrelevant since they are for yielding, which is permissable for jettison. The one remaining negative margin (-1.7% at location 31) is for the elevated temperature condition. A more accurate analysis would undoubtedly make this positive because of the various simplifying conservative assumptions used here; e.g., 1) the jettison force was assumed to act at the c.g. whereas figure 1 shows it to act considerably behind the c.g. thus reducing the bending moment at location 31; 2) the pod is assumed to be at an elevated temperature corresponding to supersonic flight whereas jettison would only occur in subsonic flight.

For carriage on the Sparrow launcher on the F-4C, the lowest margin is -0.028. This value occurs for yielding, at elevated temperatures, of the button which serves as the forward lug. For room temperature the margin is 0.002 for yielding. This button is heavily loaded because, even though the 335A pod is lighter than the Sparrow, its CG is further forward. For this critical flight load, the margins of safety for all points are given in Table XIV

This one negative margin would be positive if the larger swaybrace angles on the outboard side were used in the analysis of the lug reactions, because the large yawing moment and side load are really reacted by the outboard sway brace for this load. However, MIL-A-8591 does not have equations for unequal sway brace angles on left and right sides so the smaller angle was used to be conservative.

SECTION VIII

VIBRATION TEST DESCRIPTION AND RESULTS

8.1 TEST CONDITIONS

The pod is required by contract to meet the vibration levels specified in MIL-STD-810. The vibration environment for cycling is defined by this specification as follows:

Frequency (Hz)	Amplitude
5-14	0.10 inches D.A.
14-23	1.0g
23-52	0.036 inches D.A.
52-500	5g

For resonance dwells, the amplitude of vibration is specified to be one-half of these levels for equipment the size of the pod.

The vibration tests conducted were design evaluation tests, not qualification tests, so that the MIL-STD-810 test was used merely as a guide and modifications to it were made based on engineering judgment. Information from the McDonnell-Douglas Company indicated that vibration levels for the F-4C may be higher than those of MIL-STD-810. Because of this and because a casting formed part of the major structure, it seemed that higher input levels should be applied. The following levels were used in the test for both cycling and resonance dwells with some exceptions, described later, such as when the exciter had insufficient power.

Frequency (Hz)	Amplitude
5-14	0.10 inches D.A.
14-23	1.0g
23-74	0.036 inches D.A.
74-500	10g's

without visible damage.

8.2 RESONANCES AND AMPLIFICATIONS (Z AXIS)

In the Z-axis, there are three principal resonant frequencies: 50 Hz, 80 Hz, and 150 Hz. At the two higher frequencies, the exciter had insufficient power

(Continued on next page)

to apply the full level of 10 g's and thus delivered inputs of 8 g's at 80 Hz and 7 g's at 150 Hz. Three accelerometers were placed on the pod structure along the length; one at each end of the principal module and one on the dummy generator. The input level and the highest unfiltered output level of the three accelerometers for each resonant frequency are tabulated below:

Input (g's)	Output (g's)	Resonant Frequency (Hz)
4.5	35	50
8	30	80
7	40	150

Several minor failures occurred in the course of the first resonance dwell of vertical vibration: (1) one rib of the adapter casting cracked (see figure 9); (2) several rivets tying the aft ring to the casting loosened and one sheared (see figure 10); and (3) the screws tying the lower forward end of the heat sink to the adapter failed. The following design changes were made to improve the strength of these items: (1) the rib of the casting was given a larger cross section and its corner fillet radius was changed from a machined one-sixteenth-inch radius to an as-cast one-quarter-inch radius; (2) the rivets in the aft ring were changed from 1/8-inch to 5/32-inch diameter; and (3) the screws in the heat sink corner bracket were changed from number 10's to 1/4-inch diameter. After the changes, the vertical vibration test was begun anew and completed without failure.

8.3 TEST RESULTS (Y AXIS)

The Y-axis test was begun and the major resonances were found to be at 30, 65, and 150 Hz. The full input specified was applied at all resonance dwells and cycling was completed with no failures. The resonance dwell at 30 Hz produced one minor failure: one of the two bolts tying down the lower forward end of the heat sink sheared. This is not part of the major structure since the heat sink was still contained within the pod. The pod survived the other two resonance dwells without failure.

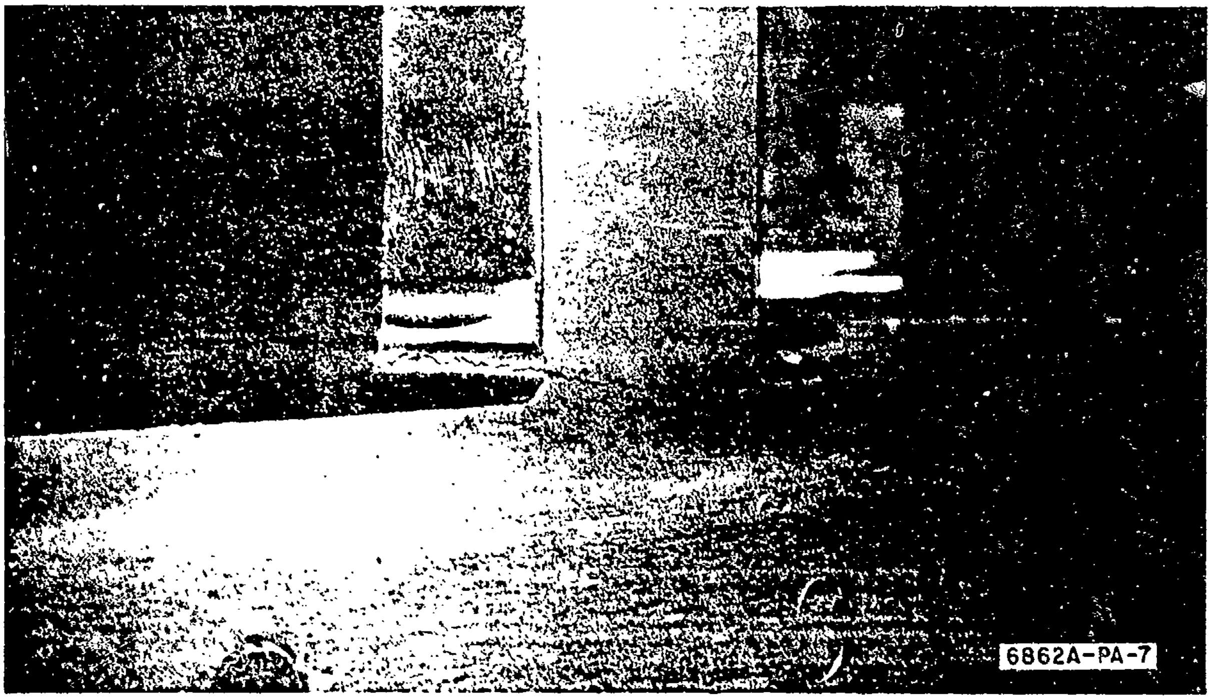

Figure 9   First Minor Failure: Cracked Rib of Adapter Casting

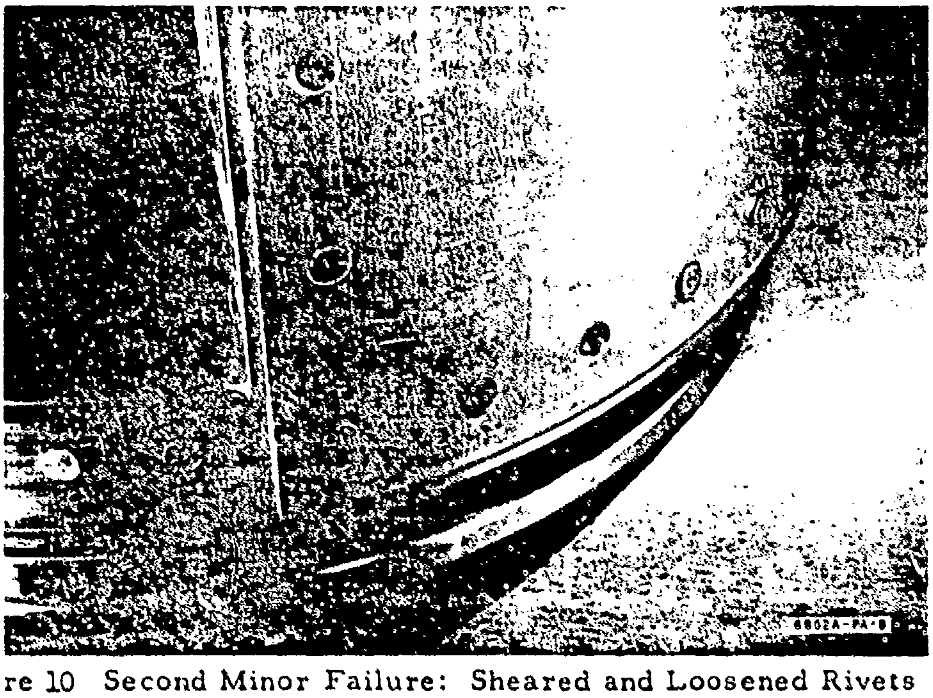

Figure 10 Second Minor Failure: Sheared and Loosened Rivets
Tying Aft Ring to Casting

8.4 CONCLUSIONS

All of the failures occurred in the adapter section, which can be attributed to very high amplifications of the heat sink (which is mounted at one end to the adapter) and to torsional oscillations of the generator. The subsequent modifications in this area (the redesigned casting, the larger rivets, and larger bolts holding the heat sink) allowed the major structure to survive all of the tests made thereafter. These changes were such as to increase the strength of those items; therefore, the tables of joint strength and margins of safety for the static load analysis are somewhat conservative for these items.

It is noteworthy that even when failures occurred, they were not immediately obvious in that the resonant frequency showed little or no noticeable shift. This indicates the high degree of redundancy of the structure which is very desirable for a structure which is apt to receive battle damage in service and yet should continue to carry the load. The levels of vibration at the resonance dwells, where the most damage typically occurs, were between two and four times the levels specified in MIL-STD-810, and the completion of these tests without damage to the primary structure is thus good proof of its adequate strength.

APPENDIX I

WEIGHT AND BALANCE

A computer program was set up to calculate the moments of inertia about the three axes and the position of the CG. Tables XXIV and XXV list the x-axis data for pods with and without generators. This data, with similar y- and z-axis data, was used in the equations shown below to calculate the moments of inertia and CG with respect to all three axes. The results are given in table XXVI.

$$X_c = \frac{\Sigma (W \overline{X})}{\Sigma W}$$

$$Y_c = \frac{\Sigma (W \overline{Y})}{\Sigma W}$$

$$Z_c = \frac{\Sigma (W \overline{Z})}{\Sigma W}$$

$$I_x = \Sigma \quad W (y_c - \overline{y})^2 + W (z_c - \overline{z})^2 \quad + \Sigma I_{0_x}$$

$$I_y = \Sigma \quad W (x_c - \overline{x})^2 + W (z_c - \overline{z})^2 \quad + \Sigma I_{0_y}$$

$$I_z = \Sigma \quad W (x_c - \overline{x})^2 + W (y_c - \overline{y})^2 \quad + \Sigma I_{0_z}$$

TABLE XXX

WEIGHT AND BALANCE DATA, X-AXIS, FOR
QRC-335A POD WITH GENERATOR

Item	W (lb)	$\bar{X}$ (in)	I_0[1] (lb-in^2)
Nose Antenna Mod	17	12.2	160
V-Clamp	3.2	17.5	77
RATG	72	26.6	1048
V-Clamp	3.2	31.8	77
Heat Sink Assy	135.5	59.8	1230
V-Clamp	3.2	41.8	77
Principal Structure	56.5	70.1	1110
V-Clamp	3.2	96.8	77
Tail Antenna Mod	12.9	102.4	153
Total	306.7		4009

TABLE XXXI

WEIGHT AND BALANCE DATA, X-AXIS, FOR
QRC-335A POD WITHOUT GENERATOR

Item	W (lb)	$\bar{X}$ (in)	I_0[1] (lb-in^2)
Nose Antenna Mod	17	12.2	160
V-Clamp	3.2	17.5	77
Heat Sink Assy	135.5	45.5	1230
V-Clamp	3.2	27.5	77
Principal Structure	56.5	55.8	1110
V-Clamp	3.2	82.5	77
Tail Antenna Mod	12.9	86.1	153
Total	231.5		2884

NOTE: Mounting Equipment: lugs, sway brace pads, etc are not included in the above tables since the equipment varies according to the particular installation. The figures for the heat sink assembly do include an allowance of 8 pounds of water in the heat sink.

TABLE XXXII

WEIGHT AND BALANCE RESULTS

Parameter	Pod With RATG	Pod Without RATG
$\bar{x}$ (in from nose)	52.54	47.83
$\bar{y}$ (in from CL)	0.101	0.134
$\bar{z}$ (in from CL)	0.186	0.246
I_x (lb-in^2 about CG)	5,064	2,983
I_y (lb-in^2 about CG)	213,906	120,728
I_z (lb-in^2 about CG)	213,542	120,366
W (lb)	306.7	231.5

MODEL RF-4C/QRC-160-8 POD FLIGHT LOADS
(SINGLE CARRIAGE AT BL = 81.50)

Condition						
Mach	1.6	0.8	1.13	1.68	1.68	1.6
Altitude (ft)	20000	10000	SL	20000	20000	20000
Maneuver	Symm	SRP	Symm	Symm	SRP	SRP
n_z (g's)	-3.0	4.8	-3.0	-3.0	4.8	4.8
p (deg/sec)	0	200	0	0	69	75
$\dot{P}$ (rad/sec^2)	0	0	0	0	0	0
Vertical						
Airload	-1650	-1035	-1270	-1415	-370	-330
Inertial Load	1350	-2870	1350	1350	-2240	-2260
Net Load	-300	-3905	80	-65	-2610	-2590
Pitching Moment	-42570	8635	-54810	-45420	-45400	-43560
Side						
Airload	-390	2545	-675	-390	2370	2180
Inertial Load	0	740	0	0	-260	-245
Net Load	-390	3285	-675	-390	2110	1935
Yawing Moment	-8350	7800	-20540	-4295	4525	4220
Rolling Moment	-1255	8080	-2130	-1250	7565	6930
Axial Load	740	160	820	790	790	740

NOTES: 1. Loads are ultimate and are in pounds and inch-pounds at the pod CG.
2. Positive directions are:
Forces: Up, outboard or aft.
Moments: Nose up, nose outboard or top inboard.
3. Pod weight is 300 pounds.

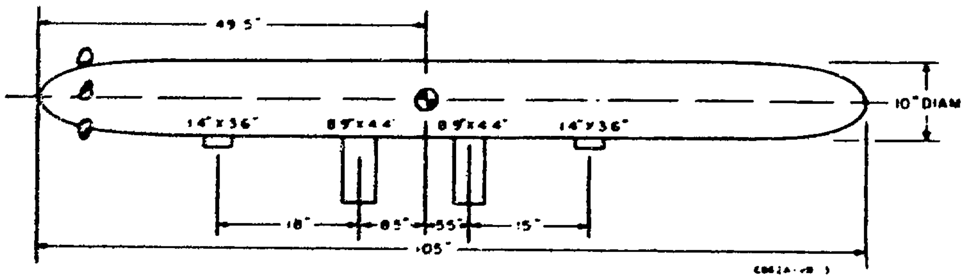

* Load Data Furnished by McDonnell Company

APPENDIX III

SPARROW III 6B LOADS FORWARD FUSELAGE INSTALLATION*

Configuration	Semisubmerged in Fuselage			
Condition				
Mach	0.64	1.92	0.76	1.82
Altitude (ft)	SL	40000	10000	40000
Maneuver	Symm	Symm	SRP	SRP
n_z (g's)	8.5	-3.0	6.6	-1.0
p (deg/sec)	0.0	0.0	260	114
$\dot{P}$ (rad/sec^2)	0.0	0.0	0.0	0.0
Loads				
Vertical				
Airload	1360	-800	630	-350
Inertial Load	-5820	2050	-5500	500
Net Load	-4460	1250	-4870	150
Pitching Moment	-16350	14200	-11930	7750
Side				
Airload	1420	-270	4150	-2390
Inertial Load	0	0	-100	1190
Net Load	1420	-270	4050	-1200
Yawing Moment	-36400	13100	-52600	40000
Rolling Moment	8200	-1530	23940	-13800
Axial Load	50	130	40	150

NOTE: 1. Ultimate values are shown.
2. Loads are in pounds, moments are in inch-pounds about weapon CG.
3. Positive directions are:
Loads: Up, outboard and aft.
Moments: Nose up, nose outboard or top inboard about missile CG.
4. Inertial Loads based on weight = 455 pounds.

*Load Data Furnished by McDonnell Company

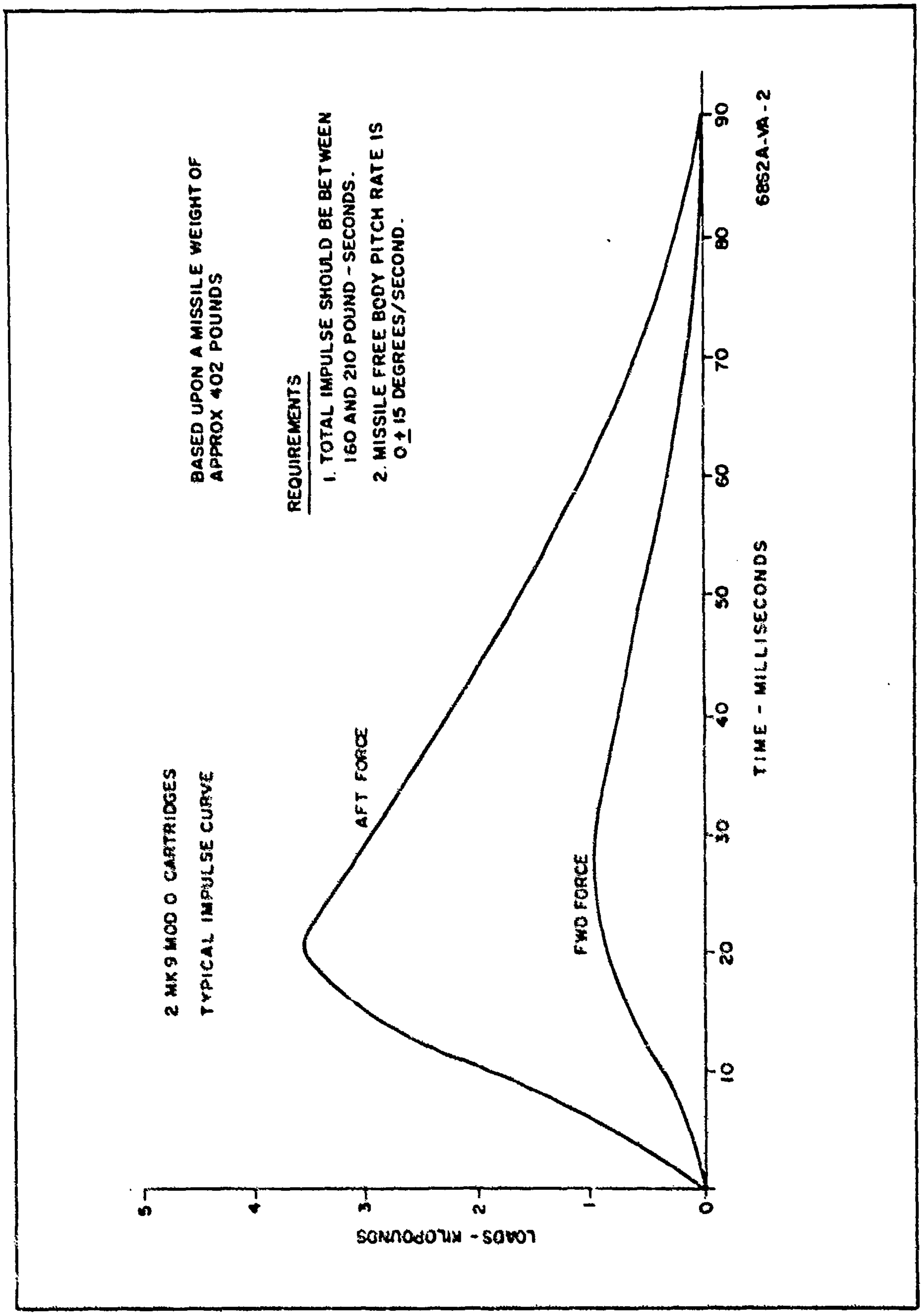

Figure 11 Typical Impulse for Jettison From Sparrow Launcher

Appendix IV

MATERIAL STRENGTHS

TABLE XXXIII

MATERIAL STRENGTHS
ROOM TEMP. (KSI)

NO.	MATERIAL.	FTY	FTU	FCY	FSU	FBRY	FBRU
1	STEEL 17-4PH	145.00	155.00	145.00	98.00	-1.00	-1.00
2	STEEL ALLOY	-1.00	-1.00	-1.00	-1.00	-1.00	-1.00
3	ALUM. 2024T3	43.00	64.50	43.00	40.00	74.00	124.00
4	ALUM. 2024T4	40.00	60.00	38.00	36.00	68.00	116.00
5	ALUM. RIVETS	-1.00	-1.00	-1.00	-1.00	-1.00	-1.00
6	ALUM. 356T61	28.00	38.00	28.00	27.00	50.00	68.00
7	ALUM. 6061T6	35.00	42.00	35.00	27.00	58.00	88.00

FRACTION OF STRENGTH AT ELEVATED TEMP.

NO.	MATERIAL.	FTY	FTU	FCY	FSU	FBRY	FBRU
1	STEEL 17-4PH	.94	.94	.94	-1.00	.93	.93
2	STEEL ALLOY	.97	.97	-1.00	.97	-1.00	-1.00
3	ALUM. 2024T3	.88	.80	.94	-1.00	.97	.93
4	ALUM. 2024T4	.88	.80	.94	.88	.97	.93
5	ALUM. RIVETS	-1.00	-1.00	-1.00	.82	-1.00	-1.00
6	ALUM. 356T61	.93	.83	.83	-1.00	-1.00	-1.00
7	ALUM. 6061T6	.88	.86	-1.00	-1.00	-1.00	-1.00

-1.00 means not required

Elevated temperature values are for exposures of 10000 hrs. at 250°F.

APPENDIX V

EQUATIONS FOR CALCULATING MOMENT CAPABILITIES OF POD JOINTS

V-BAND CLAMP AND RINGS

Sections of the pod, called modules, are joined together by V-Band clamps. A typical joint is illustrated in figure A. Before yield stresses are reached, the V-band clamp will elastically spread to allow a slight separation of the rings on the tension side. In addition, the ring itself will have some elastic distortion on the tension side. On the compression side, however, the rings are in simple compression and the V-band clamp is unleaded. As a consequence the spring constant on the compression side is far greater than the spring constant on the tension side, and the neutral axis is very close to the compression edge. This is rather analogous to a composite beam with one material having a modulus of elasticity much greater than the other. The neutral axis then moves from the center towards the side of the beam with the higher modulus of elasticity.

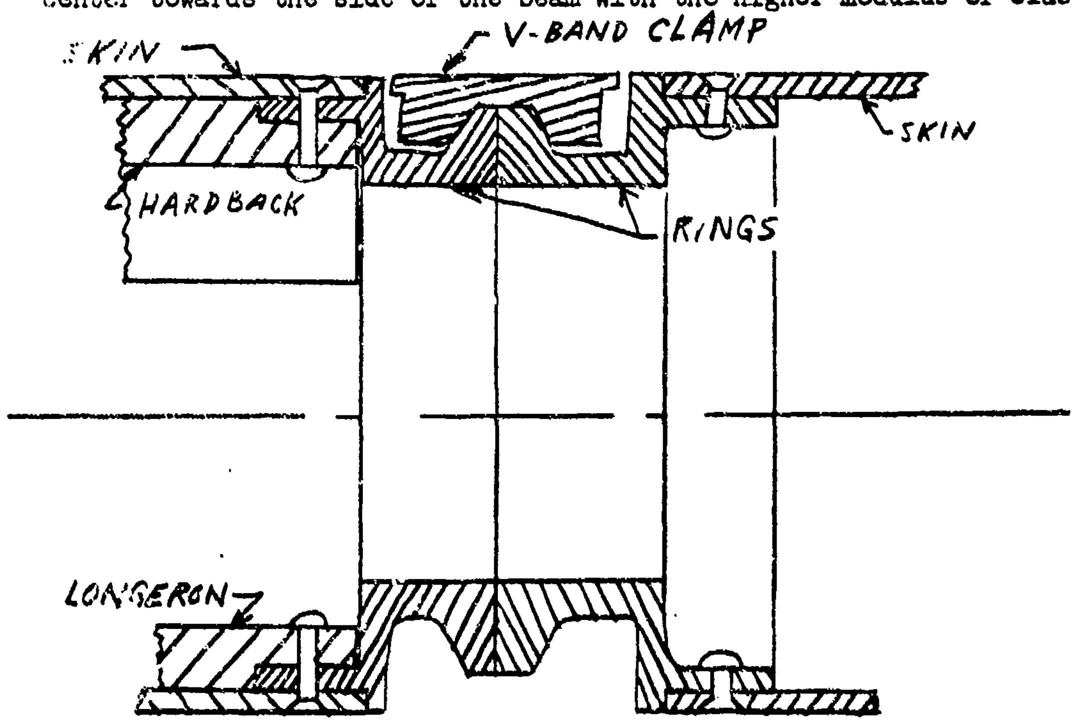

A TYPICAL JOINT

Figure A

The actual strain and force distributions around the joint will be approximately as shown below:

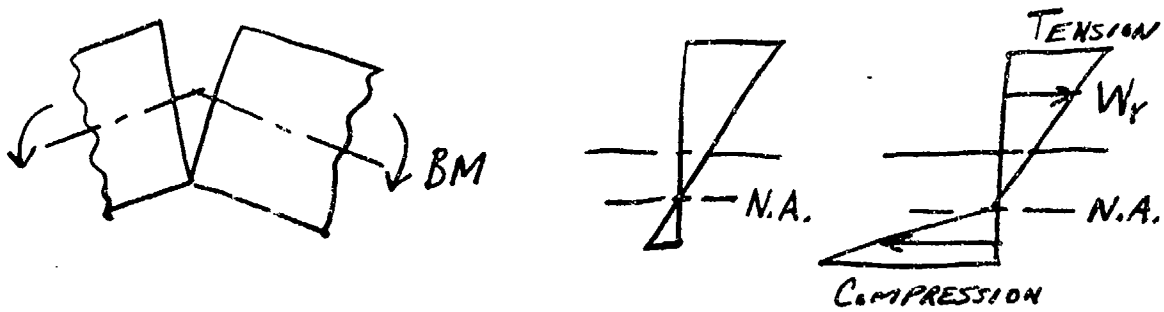

Physical Joint Strain Diagram Force Per Unit Length

For computational purposes, the force diagram will be assumed to be equivalent [illegible] diagram shown below (i.e. the neutral axis all the way to the edge). The validity of this assumption has been proven in tests as will be described later.

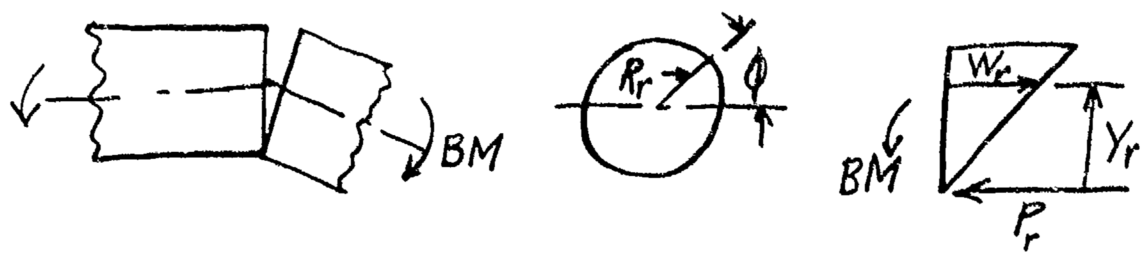

Let

W_r = longitudinal force per inch of circumference (tension)

ϕ = angle between horizontal axis and radius to a point on circumference.

W_m = maximum value of W_r

R_r = radius to effective contact between clamp and ring

Y_r = vertical distance of point above bottom

P_r = total compression force

At any point, the diagram shows that

$$W_r = W_m (1 + \sin\phi)/2$$

For equilibrium of axial forces P_r must equal the integration of the tension distribution so,

$$P_r = 2\int_{-\pi/2}^{\pi/2} (W_r R_r)\, d\phi = \pi R_r W_m$$

The mathematical model would indicate that P_r is a point load and thus the compressive stress would theoretically be infinite. Actually, of course, the neutral axis is raised slightly so that P_r is distributed over a small part of the circumference. Suppose, for example, that P_r were distributed over a three inch length of circumference (this would correspond to less than .25 inch shift in neutral axis). Then the compressive force per inch of circumference would be $\frac{\pi R_r W_m}{3.0}$ = 4.9 times as great as the maximum tensile force per inch of circumference. However, the actual stress involved is lower on the compression side, because there is no bending stress within the ring. This internal bending moment causes stresses far greater than the direct tension and compression forces, so the stresses due to P_r are lower. The internal bending stresses will be derived below.

If P_r is included, the moment of the force distribution is the same about any axis. Therefore, for convenience it will be computed about the neutral axis (bottom of the figure) where P_r adds nothing to the moment.

Integrating the tensile force distribution gives

$$BM = 2\int_{-\pi/2}^{\pi/2} W_r \; Y_r \; d\,\text{Circ}$$

$$= 2\int_{-\pi/2}^{\pi/2} W_r \; R_r \; (1 + \sin\phi) \; R_r \, d\phi$$

$$= \frac{3}{2}\pi R_r^2 \; W_m$$

The moment calculated by integrating the longitudinal forces around the circumference is numerically equal to the bending moment caused by the external pod forces. In fact, the above equation can be solved for W_m as a function of BM(bending moment). However, the computer program used for this report does not compute margins of safety by comparing actual stress with yield or ultimate stress. Instead it computes the bending moment that would initiate yielding and the bending moment that would cause rupture.

These moment capabilities are then compared with the actual bending moments to calculate the margins of safety (using appropriate factors of safety). The resulting margins of safety are exactly the same with either approach.

In order to define the maximum bending moment capability, it is necessary to calculate the limiting value for W_m. Consider a slice of the joint at the top of the ring as shown below.

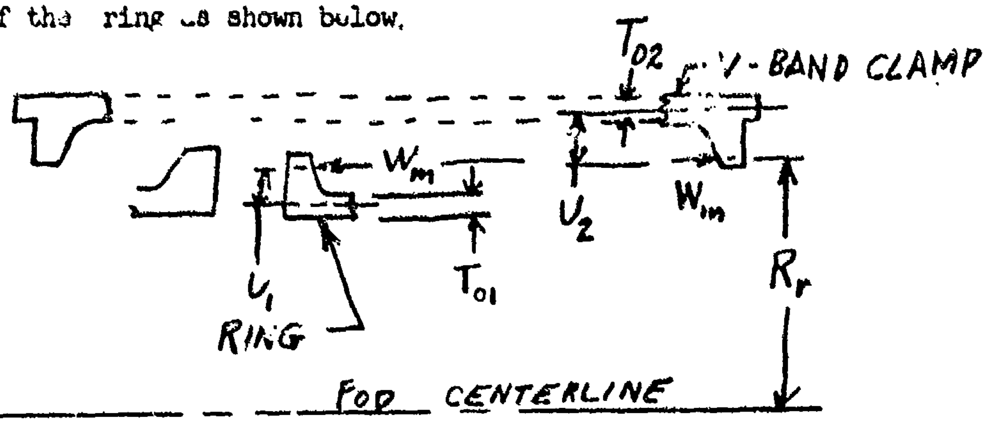

Symbols have been chosen so that the equations apply to either the V-band clamp or the ring. The critical bending stress occurs at the root of the clamp or ring (where it is broken in the diagram), because W_m has a moment arm, U, about this section.

Considering a short section of the clamp or ring that is dl long circumferentially (perpendicular to the paper), the maximum longitudinal stress at the root is the direct tension plus the tensile beam stress. The direct tensile stress is

$$S_1 = \frac{W_m \, dl}{dA} = \frac{W_m \, dl}{T_o \, dl} = W_m / T_o = W_m T_o / T_o^2$$

The bending stress is

$$S_2 = My/I = (W_m \, dl \, U)\,(T_o/2) / (T_o^3 \, dl/12)$$

$$= \frac{6W_m \, U \, dl}{T_o^2 \quad dl} = 6W_m \, U/T_o^2$$

So the total longitudinal stress is

$$S_L = W_m \, (T_o + 6\,U)/T_o^2$$

The flange of the clamp or ring prevents strain in a tangential direction. Because of Poisson's ratio, the ring would shrink tangentially if unrestrained. Therefore, a tangential stress is produced equal to

$$S_T = \mu \, S_L$$

Using the maximum shear theory of failure

$$F_t = S_L - S_T = W_m (1-\mu)\,(T_o + 6U)/T_o^2$$

where F_t = tensile strength of material (yield or ultimate).

Therefore

$$W_m = \frac{T_o^2 \quad F_t}{(1-\mu)\,(T_o + 6U)}$$

Substituting in the equation for bending moment gives the moment capability of the clamp or ring as

$$BM = \frac{3\pi R_r^2 T_o^2 F_{ty}}{2(1-\mu)(T_o + 6U)} \quad \text{for yield strength}$$

or

$$BM = \frac{3\pi R_r^2 T_o^2 F_{tu}}{2(1-\mu)(T_o + 6U)} \quad \text{for ultimate strength}$$

As an example, consider the V-band clamp. Under load, the angle of the clamp will become larger, moving the effective point of pressure towards the outside of the ring. Assuming that the effective contact point is all the way to the o.d. of the ring gives

R_r = 4.74 inch

T_o = 0.17 inch

U = 0.18 inch

μ = 0.36

F_{ty} = 145,000 psi

Then

$$BM_{(yield)} = \frac{3\pi(4.74)^2(0.17)^2(145,000)}{2(0.64)(1.25)} = 556,000 \text{ in-lb.}$$

The value of the bending moment to cause yield as caluclated from strain gage measurements during a static test of a 669A pod is 506,000 in-lb. Thus it appears that the effective contact point is not quite all the way out to the o.d. of the ring.

It is found that a value for R_r of 4.722 and a corresponding value for U of 0.198 causes the equation for BM to agree with the experimental data. Therefore, wherever the rings are steel, R_r is assumed to be 4.722 inch. Wherever the rings are aluminum, the lower modulus of elasticity of the ring will make it deflect as much or more than the V-band clamp, so in those locations the nominal midpoint (4.66 inch) of the contact area has been used for R_r.

RIVETED JOINTS

As shown in figure A, the rings are fastened to the pod skin and hardback by means of rivets or screws. Obviously, the skin is most likely to fail where it is weakened by rivet holes. There is also a possibility of the rivets failing. Therefore margins of safety are calculated based on skin tearing at the rivets, shearing of the rivets (or screws), and bearing failure at the rivets (or screws).

Rivet Shear

The following derivation represents the moment capability of a riveted joint as a function of the rivet shear stress. The derivation assumes a uniform rivet spacing. In practice this is not always true, so the capability in the vertical direction is calculated separately from the capability in the horizontal direction. In both cases, the rivet (or screw) size and spacing at the greatest distance from the neutral axis are used in the equations, because the rivet spacing near the neutral axis has very little effect. Because of the type of construction of the pod, the neutral axis will not coincide with the geometrical axis of the cylinder as shown below.

Let

X_s = distance from the cylinder axis to the neutral axis

P_r = imaginary concentrated load to balance axial forces

W_s = the longitudinal force per inch of circumference

W_m = the maximum value of W_s

R_s = radius to shear interface

ϕ = angle between horizontal axis and radius to a point on circumference

Assumed Distribution of Forces per Inch of Circumference	Actual Distribution of Forces per Inch of Circumference

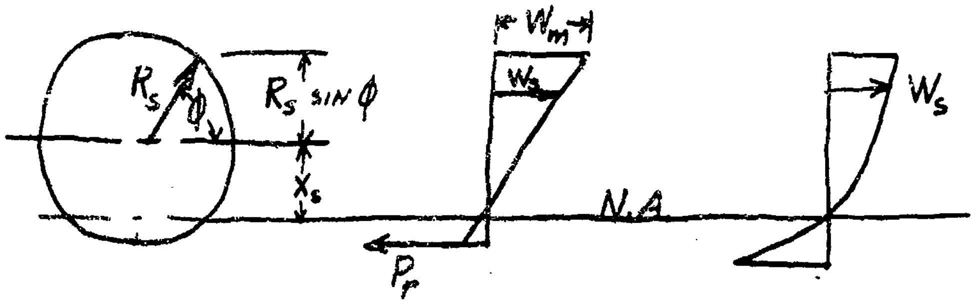

At any point on the circumference

$$W_s = \left(\frac{X_s + R_s \sin\phi}{X_s + R_s} \right) W_m$$

The force P_r is included to balance out the longitudinal forces. It is a reasonable approximation to the nonlinear distribution of longitudinal forces. This non linearity is caused partially by the end effects from the unsymmetrical forces at the V-band clamp and partially by the ridge on the rings that bears against the skin and helps to carry compressive loads. Moments can be calculated about any axis since there is no net force, so it is convenient to take moments about P_r.

Therefore

$$BM = 2\int_{-\pi/2}^{\pi/2} W_s \quad R_s \, (1 + \sin\phi) \, R_s \quad d\phi$$

$$= 2\int_{-\pi/2}^{\pi/2} W_m \left(\frac{X_s + R_s \sin\phi}{X_s + R_x} \right) (1 + \sin\phi) \, R_s^2 \quad d\phi$$

$$= \pi \, W_m \, R_s^2 \left(\frac{2\,X_s + R_s}{X_x + R_s} \right)$$

Letting

$$A\,(j) = \pi R_s^2 \left(\frac{2\,X_s + R_s}{X_s + R_s} \right)$$

Gives

$$BM_s = W_m \; A\,(j)$$

W_m is equal to the rivet (or screw) shear strength, P_s, divided by the rivet spacing, S_c, so the moment based on shearing of a single row of rivets is

$BM_s = P_s A (j)/S_c$

For most of the joints the neutral axis is assumed to be at $X_s = R_s/2$. This is based on the fact that elasticity of the V-band clamp permits the module rings to separate slightly except for a small zone on the compression side. Thus at the middle of the V-band clamp X_s nearly equals R_s. Far away from the V-band clamp $X_s = 0$ for a symentrical shell. Thus the assumption is that the end effect has diminished by fifty percent at the location of the rivets. An exception to this rule is the principal module. In the vertical direction, X_s for the principal module is assumed to be 4 inches, because the massive hardback causes X_s to be above center even where there is no end effect. At the "B" end of the principal module, where there are three rows of rivets, the horizontal value for X_s is assumed to be 1.0 inch, because there is more distance for end effects to disappear. These assumptions have been partially verified in static tests of other 669A pods.

The principal module has an additional complication due to the hardback and longeron. The bending moment is shared by the skin, hardback and longeron by the ratio of their moments of inertia about the neutral axis. Thus two bending moment capabilities can be calculated: BM_k, the moment to fail the rivets (or screws) between the ring and the skin, and BM_h, the moment to fail the screws between the ring and the hardback or longeron. The lesser of BM_k and BM_h is tabulated as the joint strength. Because the screw spacing is irregular, their actual shear strength times their average distance from the neutral axis is used. The equations for BM_k and BM_h are as follows:

Let

Q_2 = skin moment of inertia about centerline = 39 in^4

Q_3 = horizontal moment of inertia of hardback = 18 in^4

Q_4 = horizontal moment of inertia of longeron = .4 in^4

Q_5 = vertical moment of inertia of hardback about Pod Center = 82 in^4

Q_6 = vertical moment of inertia of longeron about Pod Center = 20.3 in^4

A_2 = cross section area of skin = 3.1 in^2

A_3 = cross section area of hardback = 4.84 in^2

A_4 = cross section area of longeron = 1 in^2

X_1 = vertical distance of hardback centroid from centerline = 3.98 in.

X_2 = vertical distance of longeron centroid from centerline = 4.62 in.

The moments of inertia must be translated to the neutral axis for any given X_s (in the vertical direction X_s is towards the hardback). If Q_s is the ratio of skin moment of inertia (about N.A.) to the total moment of inertia (about N.A.) and subscript 1 refers to horizontal direction and subscript 2 refers to vertical direction, then

$$Q_s(1) = \frac{Q_2+A_2 \left(X_s(1)\right)^2}{Q_2+Q_3+Q_4+A_2 \left(X_s(1)\right)^2+A_3 \left(X_s(1)\right)^2+A_4 \left(X_s(1)\right)^2}$$

$$Q_s(2) = \frac{Q_2+A_2 \left(X_s(2)\right)^2}{Q_2+Q_5+Q_6+A_2\left[X_s(2)\right]^2-A_3\left[2X_1 X_s(2)-X_s^2(2)\right]+A_4\left[2X_2 X_s(2)+X_s^2(2)\right]}$$

Letting N_w be the number of rows of rivets, the moment capability for rivet shear at the skin is

$$BM_K(j) = -\frac{N_w P_s(j)\, A(j)}{Q_s(j)\; S_c(j)}$$

j = 1 or 2 for horizontal or vertical

If N_s is the number of screws per row attaching the hardback and longeron, P_{ss} is the shear strength of the screws, and D_s is their average distance from the neutral axis, the moment capability for "rivet shear" of the screws between the ring and the hardback/longeron is

$$BM_h(j) = \frac{N_s P_{ss} D_s(j)}{1-Q_s(j)}$$

Rivet Bearing

The moment capability for rivet bearing is analogous to the calculations for rivet shear. Thus

$$BM_b = W_m A(j)$$

and $W_m = P_{br}/S_c$

and $P_{br} = F_{br} A_b$

The bearing area, A_b, is calculated as

$$A_b = (T_s - H_r/2)\, D_r$$

This assumes that the countersunk head is only half as effective in carrying bearing loads as the shank. Thus the moment for a single row of rivets is

$$BM_b(j) = C_d F_{br}(k)\, (T_s - H_r/2)\, D_r\, A(j)/S_c(j)$$

j = 1 or 2 for horizontal or vertical

k = index for skin material

where C_d = derating factor in cases where edge distance is less than twice rivet diameter

F_{br} (k) = allowable bearing stress of skin

T_s = skin thickness

H_r = head depth of rivet

D_r = diameter of rivet

A (j) = function of X_s as before

S_c = rivet spacing

P_{br} = maximum bearing force for one rivet

A_b = bearing area for one rivet

For the principal module, moment capability for bearing in the skin and for bearing in the hardback/longeron are both calculated in a manner similar to that for rivet shear. Thus

$$BM_k(j) = \frac{C_d N_w F_{br}(k) (T_s - H_r/2) D_r A(j)}{Q(j) S_c(j)}$$

For the bearing area of the screw in the hardback and longeron, the bearing area is assumed to be D_{sw}^2, where D_{sw} = screw dia, so

$$BM_h(j) = \frac{N_w N_s F_{br}(k) D_{sw}^2 D_s(j)}{1 - Q_s(j)}$$

Skin Tension

The moment capability for skin tearing is also analogous to the calculation for rivet shear. It is based on the customary assumption of a uniform stress distribution across the net area of the skin at the riveted section.

$$BM_t\ (j) = N_t\ A(j)/Q_s\ (j)$$

and $$N_t = F_{ty}\ A_t$$

and $$A_t = T_s\ (1 - Dr/S_c(j)) - D_r H_{r/2}\ S_{c(j)} = T_s - (T_s + H_{r/2})\ D_r/S_c\ (j)$$

where

A_t = the net area per unit length of circumference

N_t = force in tension per unit length of circumference

F_{ty} = yield or ultimate tensile strength of skin

Thus

$$BM_k(j) = F_{ty} \left\{ T_s - (T_s + \frac{H_r}{2})\ D_r/S_c\ (j) \right\}\ A\ (j)/Q_s\ (j)$$

APPENDIX VI

EQUATIONS FOR CALCULATING MARGIN OF SAFETY OF POD SKIN

The Westinghouse Structure Test Program, as described in reference 1, produced three sets of coefficients for computing the critical stresses in the skin of 669A type of pods. These coefficients, called CTAU, COUT, and CIN are given in Tables A, B, and C. For a given combined load case, the maximum shear stress, FT_j, at each critical location is computed as follows:

where

$CTAU_{ij}$ = longitudinal shear stress coefficient for i^{th} load component and j^{th} location from table A.

$COUT_{ij}$ = coefficient for difference between circumferential and axial stresses for i^{th} load component and j^{th} location on outside of skin from table B.

CIN_{ij} = coefficient for difference between circumferential and axial stresses for i^{th} load component and j^{th} location on inside of skin from table C.

FT_j = twice the maximum shear stress at j^{th} location caused by the total combined load. (Twice the shear stress is used because this is the number that must be compared with the tensile yield and ultimate strength.)

$$SUMOUT_j = \sum_{i=1}^{8} (COUT_{ji}) \; L_i$$

$$SUMIN_j = \sum_{i=1}^{8} (CIN_{ji}) \; L_i$$

$$SUMTAU_j = \sum_{i=1}^{8} (CTAU_{ji}) \; L_i$$

At the outside of the skin,

$$FT_j = \sqrt{(SUMOUT_j)^2 + (SUMTAU_j)^2}$$

and at the inside of the skin,

$$FT_j = \sqrt{(SUMIN_j)^2 + (SUMTAU_j)^2}$$

L_i is a vector that is generated from the net resultant loads for each case as follows:

$$L(1) = MZ/10^5 \text{ if MZ is positive, otherwise } L(1) = 0$$

$$L(2) = -MZ/10^5 \text{ if MZ is negative, otherwise } L(2) = 0$$

$$L(3) = \left(PY + \frac{MX}{R+H}\right)/10^3 \text{ if } PY + \frac{MX}{R+H} \text{ is positive, otherwise } L(3) = 0$$

$$L(4) = \left(PY + \frac{MX}{R+H}\right)/10^3 \text{ if } PY + \frac{MX}{R+H} \text{ is negative, otherwise } L(4) = 0$$

$$L(5) = PZ/10^3 \text{ if PZ is positive, otherwise } L(5) = 0$$

$$L(6) = PZ/10^3 \text{ if PZ is negative, otherwise } L(6) = 0$$

$$L(7) = \frac{MY-(R+C+E)\ PX}{10^5} \text{ if positive, otherwise } L(7) = 0$$

$$L(8) = \frac{(R+C+E)PX-MY}{10^5} \text{ if positive, otherwise } L(8) = 0$$

The test that was used to obtain the empirical coefficients did not include loads corresponding to Px and Mx. However, an inspection of the MIL-A-8591 equations shows that Mx/(R+H) affects the lug and sway brace reactions the same as P_y does, and $-(R+C+E)P_x$ affects them the same way as M_y. Thus these terms in the above equations account for the effect of P_x and M_x on the concentrated forces at the lugs and sway braces. The only thing neglected, then, is the uniformly distributed stress due to P_x or M_x. This is negligible. For example, the maximum P_x for the QRC-335A is 1113 lbs. Since the cross section area of the skin is 3.1 in^2, the uniform compressive stress due to P_x is 1113/3.1 = 360 psi. This is considerably less than 1% of the yield strength of the skin.

The factors of 10^3 or 10^5 in the denominators of L_i were used in the definitions of the coefficients to make the coefficients convenient sized numbers.

For room temperature strength, the margin of safety at each point is calculated by

$$MSY_j = \frac{KEY\ (FFY)}{SFY\ (FT_j)} - 1 \quad \text{for yield strength} \qquad \text{eq. VI-1}$$

and

$$MSU_j = \frac{KEU\ (FFU)_j}{SFU\ (FT_j)} - 1 \quad \text{for ultimate strength} \qquad \text{eq. VI-2}$$

For the elevated temperature strength, the margin of safety at each point is calculated by

$$MSYT_j = \frac{KEY\ (FFY_j)\ (CTY)}{SFU\ (FT_j)} - 1 \quad \text{for yield strength} \qquad \text{eq. VI-3}$$

and

$$MSUT_j = \frac{KEU\ (FFU_j)\ (CTU)}{SFU\ (FT_j)} - 1 \quad \text{for ultimate strength} \qquad \text{eq. VI-4}$$

where

FFY_j = room temperature tensile yield strength (43,000 psi for skin)

FFU_j = room temperature tensile ultimate strength (64,500 psi for skin)

SFY = yield safety factor = 1.15

SFU = ultimate safety factor = 1.50

CTY = degradation factor for yield strength at elevated temperatures

CTU = degradation factor for ultimate strength at elevated temperatures

KEY = empirical correlation factor for visible yielding based on rupture test = 1.64 for the skin

KEU = empirical correlation factor for rupture based on rupture test = 1.78 for the skin

Typical Skin Stress Analysis

Consider the maximum shear stress at point 13, an area near the forward sway brace of the QRC-335, for load case A2. The net resultant loads for this case are:

$PX = 1113$ lb.

$PY = 5625$ lb.

$PZ = -2721$ lb.

$MY = 88829$ in-lb.

$MZ = 3436$ in-lb.

$MX = 0$ in-lb.

$$PY + \frac{Mx}{R+H} = 5625 + 0 = 5625 \text{ lb.}$$

$$M_y - (R+C+E)\,P_x = 88829 - (5+1.7-.19)1113 = 81579 \text{ in-lb.}$$

Therefore the L_i vector for case A2 is

$$L = \begin{vmatrix} .03436 \\ 0 \\ 5.625 \\ 0 \\ 0 \\ 2.721 \\ .81599 \\ 0 \end{vmatrix}$$

For point 13, the corresponding row of COUT is $\begin{vmatrix} -1224, & -447, & -3912, & 1530 \\ -849, 256, & -9452, & 4539 \end{vmatrix}$

The matrix multiplication indicates that

$$SUMOUT_{13} = -1224(.03436)-447(0)-3912(5.625)+1530(0)-849(0)+256(2.721) -9452(.81579)+4539(0) = -29062 \text{ psi}$$

The corresponding row of CIN is

$$\begin{vmatrix} 4126, & -2491, & 4225, & -1844, & 944, & -359, & 9833, & -5059 \end{vmatrix}$$

The matrix multiplication gives

$$SUMIN_{13} = 4162(.03436) - 2491(0) + 4225(5.625) - 1844(0) + 944(0) - 359(2.721) + 9833(.81579) - 5059(0) = 30953 \text{ psi}$$

The corresponding row of CTAU is

$$\left| -530,\ 170,\ 0,\ -499,\ -277,\ 695,\ 0,\ 1716 \right|$$

The matrix multiplication gives

$$SUMTAU_{13} = -530(.03436) + 170(0) + 0(5.625) - 499(0) - 227(0) + 695(2.721) + 0(.81579) + 1716(0) = 1873 \text{ psi}$$

At the outside $FT_{13\ outs}$ $\sqrt{(-29062)^2 + (1873)^2} = 29123$ psi

At the inside $FT_{13\ inside}$ $\sqrt{(30953)^2 + (1873)^2} = 31013$ psi

Therefore,

$$MSY_{13ins} = \frac{KEY(FFY)}{SFY(FT_{13\ ins})} - 1 = \frac{1.64(43000)}{1.15\ (31013)} - 1 = .977$$

$$MSU_{13ins} = \frac{KEU(FFU)}{SFU(FT_{13\ ins})} - 1 = \frac{1.78(64500)}{1.50(31013)} - 1 = 1.482$$

$$MSYT_{13ins} = \frac{KEY(FFY)(CTY)}{SFY(FT_{13\ ins})} - 1 = \frac{1.64(43000)(.88)}{1.15\ (31013)} - 1 = .740$$

$$MSUT_{13ins} = \frac{KEU(FFU)(CTU)}{SFY(FT_{13\ ins})} - 1 = \frac{1.78(64500)(.80)}{1.50(31013)} - 1 = .985$$

TABLE A

NO	+MZ	-MZ	+PY	-PY	+PZ	-PZ	+MY	-MY
11	-463.	860.	-849.	1150.	-0.	535.	870.	2425.
12	-860.	463.	-1150.	849.	0.	-535.	-870.	-2425.
13	-530.	170.	0.	-499.	-227.	695.	-0.	1716.
14	-170.	530.	499.	-0.	227.	-695.	0.	-1716.
15	-436.	1501.	0.	-0.	45.	-261.	-650.	2461.
16	-1501.	436.	0.	-0.	-45.	261.	650.	-2461.
17	-2151.	-532.	-2401.	-0.	-288.	85.	-604.	343.
18	532.	2151.	0.	2401.	288.	-85.	604.	-343.
19	-0.	-925.	-2393.	-0.	-511.	113.	-633.	-3941.
20	925.	0.	0.	2393.	511.	-113.	633.	3941.

CTAU
SKIN STRESS COEFICIENTS

TABLE B

NO	+MZ	-MZ	+PY	-PY	+PZ	-PZ	+MY	-MY
11	-2554.	-617.	-3207.	1040.	-694.	198.	-8383.	2575.
12	-617.	-2554.	1040.	-3207.	-694.	198.	-8383.	2575.
13	-1224.	-447.	-3912.	1530.	-849.	256.	-9452.	4539.
14	-447.	-1224.	1530.	-3912.	-849.	256.	-9452.	4539.
15	807.	-3257.	-3216.	2117.	-1580.	1115.	8563.	-14520.
16	-3257.	807.	2117.	-3216.	-1580.	1115.	8563.	-14520.
17	1542.	-4215.	-3127.	1927.	-1467.	1052.	8048.	-14569.
18	-4215.	1542.	1927.	-3127.	-1467.	1052.	8048.	-14569.
19	3676.	-2694.	-2382.	2576.	-935.	1299.	8304.	-7183.
20	-2694.	3676.	2576.	-2382.	-935.	1299.	8304.	-7183.

COUT

SKIN STRESS COEFICIENTS

TABLE XIV C

NO	+MZ	-MZ	+PY	-PY	+PZ	-PZ	+MY	-MY
11	5910.	-2739.	3488.	-1320.	786.	-292.	8839.	-3047.
12	-2739.	5910.	-1320.	3488.	786.	-292.	8839.	-3047.
13	4162.	-2491.	4225.	-1844.	944.	-359.	9833.	-5059.
14	-2491.	4162.	-1844.	4225.	944.	-359.	9833.	-5059.
15	-5362.	7812.	4104.	-3006.	1708.	-1248.	-9228.	15134.
16	7812.	-5362.	-3006.	4104.	1708.	-1248.	-9228.	15134.
17	-5953.	8626.	4080.	-2880.	1588.	-1173.	-8659.	15172.
18	8626.	-5953.	-2880.	4080.	1588.	-1173.	-8659.	15172.
19	-8281.	7299.	3377.	-3571.	1024.	-1389.	-8757.	7630.
20	7299.	-8281.	-3571.	3377.	1024.	-1389.	-8757.	7630.

CIN
SKIN STRESS COEFICIENTS

REFERENCES

1. Final Report, Structure Test Program, 669A Pods, Technical Report AFSC-TR-66, July 1966, for Headquarters Systems Engineering Group, Air Force Systems Command, Wright Patterson Air Force Base, Ohio.

2. General Design Criteria for Airborne Stores and Associated Equipment, MIL-A-8591C, 30 March 1961.

3. Interface of ECM pads with Tactical Aircraft, Technical Report SEG-TR-66-49, October 1966, for Headquarters Systems Engineering Group, Air Force Systems Command, Wright-Patterson Air Force Base, Ohio. (or later edition-SEG-TR-67-23)

SUPPLEMENTARY

INFORMATION

Missing Pages attached

AD-A068560

STRESS AND FATIGUE ANALYSIS
QRC-335A POD

Revision C

NOV 10 1[illegible]

Albert B. Simon

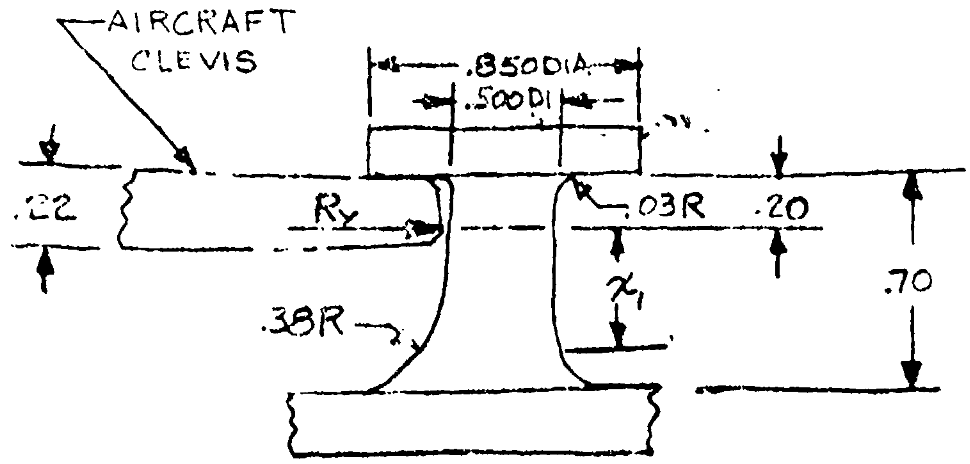

SHOWING CLEVIS, BUTTON, POSITION OF R_y AND x_1.

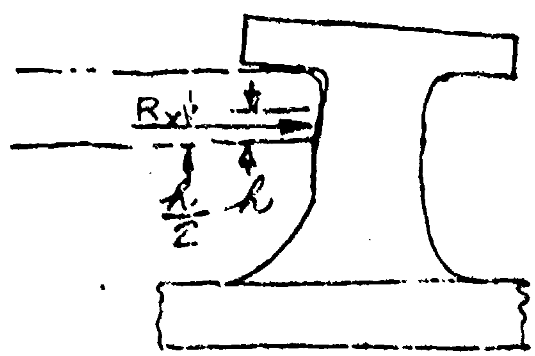

SHOWING DEFLECTION OF BUTTON AND DEFORMATION OF CLEVIS DUE TO R_y

Figure 7

TABLE XXII (Cont.)

QRC335 +GEN.VERTICAL MOMENT (LIMIT LOADS)

Load Case	STA. FOR MAX	MAX VALUE	JOINT1 X= 17.5	JOINT2 X= 31.8	JOINT3 X= 41.8	JOINT4 X= 96.8
A 1	67	-57247	43	-2661	-6235	-2897
A 2	67	-48042	797	2764	4992	-2564
A 3	70	34802	-778	-2623	-4874	2283
A 4	53	-47674	-1198	-8104	-16779	-219
A 5	53	-29032	-595	-5163	-10678	-781
A 6	53	-26929	-1139	-5630	-11568	1209
B 1	53	-21846	43	-2661	-6235	-2897
B 2	58	43287	797	2764	4992	-2564
B 3	78	20875	-778	-2623	-4874	2283
B 4	53	-33483	-1198	-8104	-16779	-219
B 5	53	-19706	-595	-5163	-10678	-781
B 6	53	-28086	-1139	-5630	-11568	1209
C 9	53	-18564	-728	-3366	-7136	532
C10	53	-37075	-973	-6941	-14601	-792
C11	53	-22446	-848	-3971	-8269	840
C12	53	-17928	-718	-3290	-6922	637
C13	53	-45645	-1560	-9689	-19961	410
C14	53	-44178	-1525	-9503	-19573	385
D 9	47	-14097	-728	-3366	-7136	532
D10	47	-20520	-973	-6941	-14601	-792
D11	47	-15993	-848	-3971	-8269	840
D12	47	-[illegible]4073	-718	-3290	-6922	637
D13	47	-31186	-1560	-9689	-19961	410
D14	47	-30366	-1525	-9503	-19573	385
G 7	51	176632	7153	51462	106505	3160

QRC335 WELLVERTICAL MOMENT (LIMIT LOADS)

Load Case	STA. FOR MAX	MAX VALUE	JOINT1 X= 17.5	JOINT2 X= 27.5	JOINT3 X= 82.5
E15	56	-41096	-491	-2626	-521
E16	31	1430	204	1008	-75
E17	56	-154412	-791	-3787	-1432
E18	56	-78080	-110	-371	705
F 8	47	-18447	-644	-1720	2958

This table is the same as that specified in MIL-STD-810 below 52Hz. Above that frequency, the vibration level is higher and becomes twice the amplitude above 74Hz for frequency sweeps. For resonance dwells, the input level was twice the level specified by MIL-STD-810 for low frequencies and four times the level at high frequencies.

The test method specified by MIL-STD-810 for qualification tests entails 3 hours of vibration for each of three axes, and these three hours are divided into half-hour dwells at major resonances with the remainder of the time cycling over the specified range of frequencies. Because of fixture limitations, vibration tests could only be conducted for two axes: the Y (side-to-side) axis and the Z (vertical) axis. Thus, the time of vibration for each axis was increased to 4.5 hours to give the same total time for the vibration test. The configuration tested was that shown in Fig. 1, because, being the longest and heaviest configuration, it is the most highly stressed. Furthermore, the adapter casting could be checked in this configuration.

Examination of the input and output vibration levels, monitored by accelerometers, showed that the response of the structure was far from sinusoidal. When the output was filtered with a 10 Hz bandpass filter, the amplitude was typically only about one-half to one-fourth of the unfiltered response indicating that many higher harmonics were excited. At some frequencies, the force feedback of the structure was so great as to make it impossible for the machine to apply the full intended level. It was also difficult at times to define precisely a resonant frequency because of the complex mode shapes and the degree of off-axis response. This is due partly to the method of support using sway braces which lift off the surface under severe responses, in part to the heat sink which is semi-floating in the shell, and in part to the torsional responce of the structure to translational inputs. Because of these difficulties, an analytical approach to the fatigue analysis becomes impractical, and the design of the primary structure is proven by having it survive the very severe vibration endurance test